Published in final edited form as:

Cell Host Microbe. 2018 April 11; 23(4): 485–497.e5. doi:10.1016/j.chom.2018.03.010.

The Receptor-like Cytoplasmic Kinase BIK1 Localizes to the Nucleus and Regulates Defense Hormone Expression during Plant Innate Immunity

Neeraj K. Lal[1,*], **Ugrappa Nagalakshmi**[2,8], **Nicholas K. Hurlburt**[3,8], **Rosalva Flores**[1], **Aurelie Bak**[4], **Pyae Sone**[4], **Xiyu Ma**[5], **Gaoyuan Song**[6], **Justin Walley**[6], **Libo Shan**[7], **Ping He**[5], **Clare Casteel**[4], **Andrew J. Fisher**[3,*], and **Savithramma P. Dinesh-Kumar**[1,9,*]

[1]Department of Plant Biology and The Genome Center, College of Biological Sciences, University of California, Davis, Davis, CA 95616, USA

[2]Department of Plant Biology, College of Biological Sciences, University of California, Davis, Davis, CA 95616, USA

[3]Departments of Chemistry, and Molecular and Cellular Biology, University of California, Davis, Davis, CA 95616, USA

[4]Department of Plant Pathology, College of Agricultural and Environmental Sciences, University of California, Davis, Davis, CA 95616, USA

[5]Department of Biochemistry and Biophysics and Institute for Plant Genomics and Biotechnology, Texas A&M University, College Station, TX 77843, USA

[6]Department of Plant Pathology and Microbiology, Iowa State University, Ames, IA 50011, USA

[7]Department of Plant Pathology and Microbiology and Institute for Plant Genomics and Biotechnology, Texas A&M University, College Station, TX 77843, USA

[8]These authors contributed equally

[9]Lead Contact

SUMMARY

[*]Correspondence: nkrlal@ucdavis.edu (N.K.L.), ajfisher@ucdavis.edu (A.J.F.), spdineshkumar@ucdavis.edu (S.P.D.-K.).

AUTHOR CONTRIBUTIONS

N.K.L. and S.P.D.-K. conceived the study and designed the experiments. N.K.L. and S.P.D.-K. crystallized the protein. A.J.F., N.K.H., N.K.L., and S.P.D.-K. determined the structure. N.K.L. performed biochemistry experiments. G.S. and J.W. performed MS analyses. N.K.L., U.N., and R.F. generated and analyzed transgenic plants. U.N. performed microscopy and qRT-PCR work. N.K.L., A.B., P.S., and C.C. determined hormone levels. X.M., L.S., and P.H. performed BIK1 and mutants interaction with EFR. All authors discussed the data. N.K.L., A.J.F., and S.P.D.-K. wrote the manuscript.

SUPPLEMENTAL INFORMATION

Supplemental Information includes six figures and two tables and can be found with this article online at https://doi.org/10.1016/j.chom.2018.03.010.

DECLARATION OF INTERESTS

The authors declare no competing interests.

SUPPORTING CITATIONS

The following reference appears in the Supplemental Information: Robert and Gouet (2014).

Plants employ cell-surface pattern recognition receptors (PRRs) to detect pathogens. Although phytohormones produced during PRR signaling play an essential role in innate immunity, a direct link between PRR activation and hormone regulation is unknown. EFR is a PRR that recognizes bacterial EF-Tu and activates immune signaling. Here we report that EFR regulates the phytohormone jasmonic acid (JA) through direct phosphorylation of a receptor-like cytoplasmic kinase, BIK1. The BIK1 structure revealed that the EFR-phosphorylated sites reside on a uniquely extended loop away from the BIK1 kinase core domain. Phosphomimetic mutations of these sites resulted in increased phytohormones and enhanced resistance to bacterial infections. In addition to its documented plasma membrane localization, BIK1 also localizes to the nucleus and interacts directly with WRKY transcription factors involved in the JA and salicylic acid (SA) regulation. These findings demonstrate the mechanistic basis of signal transduction from PRR to phytohormones, mediated through a PRR-BIK1-WRKY axis.

In Brief

Receptor-like cytoplasmic kinases (RLCKs) function at the plasma membrane during plant pattern recognition receptor (PRR)-mediated immunity. Lal et al. show that the RLCK BIK1 is uniquely phosphorylated by the PRR EFR and localizes to the nucleus where it interacts with WRKY transcription factors to regulate defense hormones during plant immunity.

Graphical Abstract

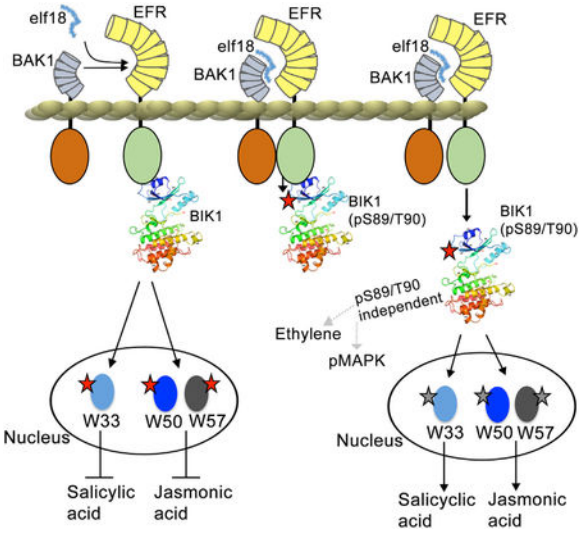

INTRODUCTION

The cell-surface-localized pattern recognition receptors (PRRs) that recognize conserved pathogen-associated molecular patterns (PAMPs) form the first layer of defense against invading pathogens in plants (Couto and Zipfel, 2016). In *Arabidopsis thaliana*, flagellin-sensitive 2 (FLS2) and EF-Tu receptor (EFR) PRRs recognize PAMPs associated with bacteria and provide broad-spectrum resistance against bacterial pathogens (Gómez-Gómez and Boller, 2000; Zipfel et al., 2006). FLS2 and EFR receptor kinases detect a highly conserved N-terminal 22-amino-acid region of bacterial flagellin (flg22) and 18-amino-acid

region of bacterial translation elongation factor Tu (EF-Tu) (elf18), respectively. The flg22 PAMP acts as molecular glue between the extracellular leucine-rich repeat (LRR) region of FLS2 and its co-receptor brassinosteroid-insensitive 1 (BRI1)-associated kinase 1 (BAK1) to establish an active immune receptor complex (Sun et al., 2013). The intracellular kinase domain of BAK1 and PRR undergoes a series of trans-phosphorylation events that lead to activation of PAMP-triggered immunity (PTI) (Yan et al., 2012).

Arabidopsis Botrytis-induced kinase 1 (BIK1) is a member of the receptor-like cytoplasmic kinase (RLCK) family (Veronese et al., 2006) that plays an important role downstream of PRRBAK1 complex. BIK1 directly interact with BAK1 and associate with PRRs in the absence of PAMP (Lu et al., 2010; Zhang et al., 2010). BIK1 and BAK1 can trans-phosphorylate each other at conserved auto-phosphorylation sites *in vitro* (Lin et al., 2014; Lu et al., 2010). BAK1 also functions as a co-receptor for PEP1 receptor that recognizes endogenous AtPep1 and brassinosteroid hormone receptor (BRI1) (Li et al., 2002; Nam and Li, 2002; Postel et al., 2010). Since BAK1 is a shared co-receptor of many plasma membrane localized receptors, its activation and trans-phosphorylation of BIK1 would not provide specificity for PRR signaling. Furthermore, kinase domains of EFR and FLS2 PRRs have been shown to possess weak or undetectable auto- and no trans-phosphorylation activities (Gómez-Gómez et al., 2001; Schwessinger et al., 2011). The specific trans-phosphorylation event on BIK1 leading to activation of downstream signaling event remains unclear, as BAK1 only trans-phosphorylate BIK1 on conserved auto-phosphorylation sites and PRR shows no trans-phosphorylation toward BIK1 (Lin et al., 2014; Schwessinger et al., 2011).

Upon PAMP perception, BIK1 is dissociated from PRR complex and is involved in downstream activation of immune signaling (Lu et al., 2010; Zhang et al., 2010). However, direct targets of BIK1 downstream of PRR complex remain largely unknown. Plasma membrane localized *Arabidopsis* respiratory burst oxidase homolog D (RBOHD) belonging to NADPH oxidase family is primarily responsible for PAMP-induced reactive oxygen species (ROS) (Nühse et al., 2007). Post-PAMP perception, BIK1 directly interact and phosphorylate RBOHD at S39, S339, and S343 sites to modulate ROS level (Kadota et al., 2014; Li et al., 2014).

Phytohormones play an important role in immune signaling and establishment of long-term resistance (Pieterse et al., 2012). Jasmonic acid (JA) and ethylene (ET) are mostly involved in resistance against necrotrophic pathogens, while salicylic acid (SA) is involved in providing resistance against biotrophic and hemibiotrophic pathogens (Glazebrook, 2005; Robert-Seilaniantz et al., 2011). Interestingly, SA, JA, and ET levels are increased upon flg22 perception (Felix et al., 1999; Flury et al., 2013; Mishina and Zeier, 2007) and play positive roles in PTI (Hillmer et al., 2017; Kim et al., 2014; Tsuda et al., 2009; Zipfel et al., 2004). However, the mechanism through which PAMP perception at the plasma membrane leads to activation of hormone responses remains unclear.

Here, we show that EFR can directly phosphorylate BIK1 to regulate JA and SA levels. Phosphonull mutation of these sites on BIK1 abolishes elf18-mediated seedling growth inhibition. Crystal structure of BIK1 revealed that these sites reside on a uniquely extended

loop at the N terminus of BIK1. Phosphomimetic mutation at EFR-mediated BIK1 phosphorylation sites resulted in constitutively elevated level of JA, which further increases significantly with bacteria *Pseudomonas syringae* pv. *tomato* (*Pst*) DC3000 infection. We found that BIK1, in addition to being present in the plasma membrane, also localizes to the nucleus and interacts with WRKY transcription factors (TFs) involved in JA and SA regulation. Our study provides evidence for a new branch of immune signaling during bacterial infection involving plant hormone JA. Our finding of BIK1's presence in the nucleus and its interaction with TFs revealed a mechanism of this pathway from plasma membrane localized PRRs to the nuclear localized TFs.

RESULTS

EFR Directly Phosphorylates BIK1

To investigate if a PRR can directly phosphorylate BIK1, we performed *in vitro* kinase assays using purified proteins. Previously it has been shown that the cytoplasmic domain of PRR purified from *Escherichia coli* possesses weak auto- and trans-phosphorylation activity (Schwessinger et al., 2011). However, this could be due to improper folding of eukaryotic protein purified from a prokaryotic expression system. Lack of a purified, active PRR kinase protein has prevented a detailed molecular characterization of early events of PRR signaling. To circumvent this, we purified the cytoplasmic domain of EFR (EFR_CD) using a eukaryotic insect cell expression system. Interestingly, EFR_CD purified from insect cell expression system displayed robust auto- and trans-phosphorylation activity toward BIK1 (Figure 1A, lane 2), while kinase-dead EFR_CD* has impaired kinase activity (Figure 1A, lane 3). Human epidermal growth factor receptor and other mammalian receptor kinases require a juxtamembrane (JM) region for kinase activity (Thiel and Carpenter, 2007). However, the importance of JM region in PRR kinase activity is not known. We found that JM region of EFR is required for both auto- and trans-phosphorylation activity as EFR cytoplasmic domain lacking JM region (EFR_CDDJM) displayed diminished auto-phosphorylation and trans-phosphorylation toward BIK1 (Figure 1A, lane 4). These results were further confirmed by a radioactive-based kinase assay (Figure 1B). These findings demonstrate that EFR cytoplasmic domain has robust kinase activity and can directly phosphorylate BIK1, establishing a direct PRR to RLCK phosphorelay.

To determine the region of BIK1 trans-phosphorylated by EFR_CD, we performed mass spectrometry analysis and repeatedly found four amino acid residues of BIK1 being phosphorylated; S89, T90, T120, and S129 (Figures 1C and S1).

BIK1 S89 and T90 Are Important for EFR-Mediated Seedling Growth Inhibition

To test the function of BIK1 residues phosphorylated by EFR, we mutated the identified Ser (S) and Thr (T) residues with Ala (A), which lacks phosphorylatable hydroxyl group. We generated transgenic *Arabidopsis* lines with wild-type genomic BIK1 ($BIK1^{WT}$), BIK1 S89A and T90A ($BIK1^{S89A/T90A}$), BIK1 T120A ($BIK1^{T120A}$), BIK1 S129A ($BIK1^{S129A}$), and BIK1 T120A and S129A ($BIK1^{T120A/S129A}$) under the control of BIK1 native promoter in the *bik1* background (Lu et al., 2010; Veronese et al., 2006). Seedling growth inhibition in the presence of elf18 peptide ligand is a commonly used assay for screening mutants with

dysfunctional EFR signaling (Zipfel et al., 2006). Among the four BIK1 mutant lines tested, only BIK1$^{S89A/T90A}$ showed insensitivity toward elf18-mediated growth inhibition (Figures 2A, S2A, and S2B), demonstrating the functional importance of S89/T90 in elf18-mediated EFR signaling.

Mutation to Asp(D) can mimic the negative charge of phosphorylated Ser/Thr and has a potential to act like a gain-of-function mutation exhibiting the constitutively phosphorylated state. Therefore, we generated stable transgenic *Arabidopsis* lines with BIK1 S89D and T90D mutations (BIK1$^{S89D/T90D}$) under the control of BIK1 native promoter in the *bik1* background. Interestingly, BIK1$^{S89D/T90D}$ seedlings were hypersensitive to elf18-mediated growth inhibition compared with Col-0 and BIK1$^{S89A/T90A}$ seed lings (Figure 2B, S2C, and S2D). The elf18 insensitivity of BIK1$^{S89A/T90A}$ was on par with that of *bak1–5* (Figure 2B), which was identified as a point mutation of BAK1 co-receptor with severely impaired PRR signaling (Schwessinger et al., 2011). These results indicated that BIK1 S89 and T90 play an important role during EFR signaling.

BIK1 Crystal Structure Revealed a Uniquely Extended b Loop that Contains S89 and T90 Residues

To understand the importance of S89/T90 and map these sites on the three-dimensional structure, we determined the crystal structure of BIK1 at 2.35Å resolution (Lal et al., 2016) (Table S1). BIK1 displays similar structure and topology to the canonical Ser/Thr and Tyr kinases (Figure 3A) (Hanks and Hunter, 1995; Wei et al., 1994). The crystallographic asymmetric unit contains two monomers with 1,100Å2 buried surface area, suggesting a weak crystallization-induced dimer rather than a biologically relevant one (Figure S3A). Consistent with this, BIK1 exists as a monomer in solution as demonstrated by gel filtration data (Figure S3B).

The S89/T90 residues lie in the β2-β3 loop, which is significantly longer than other homologous kinases (Figures 3B, 3C, and S3C–S3E). Superposition of BIK1 structure onto similar kinases BAK1 (PDB: 3uim), BRI1 (PDB: 4oa9), and IRAK4 (PDB: 2nry), reveals that the β2-β3 loop is uniquely extended compared with other kinases (Figures 3B, 3C, and S3E). In all other kinases, the β2-β3 loop is short and forms a b hairpin turn, but, in BIK1, the loop is 10 residues longer and forms more of an open “flower” creating a platform that may be involved in interaction with downstream PRR signaling proteins (Figures 3B, 3C, and S3C–S3E). The S89/T90 residues are present outside the core catalytic/activation loop (Figure 3D), hence the kinase activity of BIK1 was not affected by S89A/T90A mutations (Figure S3F).

The superposition of BIK1 also reveals that helix αC lies in a different orientation compared with BAK1, BRI1, and IRAK4 kinases, where it is shifted away from the active site (Figure S3G). This helix, which corresponds to the “PSTAIRE helix” in cyclin-dependent kinases (CDKs) (Huse and Kuriyan, 2002), has a disposition similar to the inactive CDKs. This helix in CDK, which contains catalytically important Glu51, shifts into an active conformation upon binding cyclin (Jeffrey et al., 1995) (Figure S3H), suggesting that our BIK1 structure may be in an inactive conformation and may interact with other cellular factor(s) to push the helix into an active conformation.

BIK1$^{S89D/T90D}$ Mutant Exhibits Enhanced Resistance to *Pst* DC3000 Bacteria

The *bik1* plants show growth defect phenotype due to its dual role in defense and growth (Laluk et al., 2011; Veronese et al., 2006). Mutations in the activation loop of BIK1, which compromises BIK1 kinase activity, cannot rescue *bik1* growth defect phenotype (Lin et al., 2014), suggesting that BIK1 enzymatic activity is required for growth. Interestingly, while BIK1^{WT} and BIK1$^{S89A/T90A}$ completely rescued *bik1* growth defect phenotype, BIK1$^{S89D/T90D}$ exacerbated the phenotype (Figures 4A, S4A, and S4B). It is important to note that the BIK1 kinase activity is not affected by mutations at S89 and T90 (Figure S4C), indicating that the enhanced growth defect phenotype of BIK1$^{S89D/T90D}$ is not due to the effect on kinase activity. These results suggest a signaling specific role of these mutations without affecting the enzymatic property of BIK1.

The aspartic acid at position 87 (D87) and glutamic acid at 88 (E88) give a partial negative potential to the area surrounding S89/T90 (Figure 4B). Phosphorylation at S89/T90 likely makes this region further negatively charged (Figure 4C) and might modulate its interaction with PRR complex or downstream components involved in immunity. BIK1 has been shown to dissociate from PRR complex post-ligand recognition. Protein phosphorylation can play an important role in protein-protein interaction due to enhanced negative electrostatic charge by phosphorylation. Therefore, we tested the association between BIK1^{WT}, BIK1$^{S89A/T90A}$, and BIK1$^{S89D/T90D}$ with EFR in *Arabidopsis* protoplasts by co-immunoprecipitation assay. BIK1$^{S89D/T90D}$ association with EFR was significantly reduced in the presence and absence of elf18 peptide (Figure S4D), suggesting that activated BIK1 has weaker interaction with EFR complex *in vivo*.

To determine the effect of mutations, we infected BIK1$^{S89A/T90A}$, BIK1$^{S89D/T90D}$, and control Col-0 plants with *Pst* DC3000 bacteria. BIK1$^{S89A/T90A}$ plants were more susceptible to *Pst* DC3000 infection, while BIK1$^{S89D/T90D}$ plants were more resistant than Col-0 plants (Figures 4D and 4E). A detailed time course analyses of infection revealed that enhanced resistance in BIK1$^{S89D/T90D}$ starts as early as 1 day post-infection (Figure S4E). The *bik1* mutant has been shown to be more resistant to *Pst* DC3000 due to increased levels of SA (Veronese et al., 2006). In addition, BIK1$^{S89D/T90D}$ plants pretreated with elf18 showed further decrease in bacterial growth (Figure 4F). Together, these results demonstrate that phosphonull mutation at S89/T90 is a loss-of- function mutation that makes BIK1$^{S89A/T90A}$ insensitive to elf18-mediated immune responses and susceptible to *Pst* DC3000 infection. On the other hand, phosphomimetic BIK1$^{S89D/T90D}$ is a gain-of-function mutation that makes plants hypersensitive to elf18-mediated immune responses and enhanced resistant to *Pst* DC3000 infection.

Defense Phytohormone JA and SA Levels Are Elevated in BIK1$^{S89D/T90D}$ Plants

Next, we explored the underlying mechanism of BIK1$^{S89D/T90D}$ activation of EFR signaling. Since mitogen-activated protein kinases (MAPKs) are activated during EFR-mediated signaling, we tested MAPK activation in BIK1$^{S89A/T90A}$ and BIK1$^{S89D/T90D}$ plants. BIK1$^{S89A/T90A}$ and BIK1$^{S89D/T90D}$ both showed dynamic activation of MAPK phosphorylation similar to Col-0 wild-type in response to elf18 (Figure S5A). This is consistent with the finding that BIK1 does not play a role in MAPK cascade activation

during PTI, as *bik1* plants have normal MPK3/6 activation dynamics in response to elf18 (Ranf et al., 2014).

BIK1 is a multifunctional protein and plays an important role in hormone regulation in addition to its role in PRR signaling (Laluk et al., 2011; Veronese et al., 2006). The plant hormones JA, ET, and SA play important roles during immune signaling post-pathogen recognition (Hillmer et al., 2017; Pieterse et al., 2012; Robert-Seilaniantz et al., 2011; Tsuda et al., 2009). However, a direct mechanistic link connecting PRR signaling to hormone activation is missing.

BIK1 is a positive regulator of ET pathway as *bik1* plants are insensitive to ET and its precursor 1-aminocyclopropane-1-carboxylic acid (ACC) (Laluk et al., 2011). Therefore, we tested if mutations at S89/T90 affect the ET response. Both BIK1$^{S89A/T90A}$ and BIK1$^{S89D/T90D}$ mutations lead to restoration of *bik1* phenotype to Col-0 wild-type level in response to ACC treatment (Figures 5A and 5B). ET and JA have been shown to play a synergistic role in defense (Pieterse et al., 2012); however, JA has not been shown to be involved during bacterial resistance. We next asked if JA levels are affected in BIK1$^{S89A/T90A}$ and BIK1$^{S89D/T90D}$ plants. Interestingly, JA levels were increased in non-infected BIK1$^{S89D/T90D}$ plants compared with BIK1$^{S89A/T90A}$, *bik1*, and Col-0 (Figure 5C). In addition, the JA levels further increase significantly following infection with *Pst* DC3000 in BIK1$^{S89D/T90D}$ (Figures 5D and S5B). Interestingly, even SA levels were increased in non-infected BIK1$^{S89D/T90D}$ plants and significantly increased in BIK1$^{S89D/T90D}$ plants infected with *Pst* DC3000 (Figures 5E and S5C). The SA level at 24 hr post-infection (hpi) in BIK1$^{S89D/T90D}$ mutant is similar to SA level at 48 hpi in Col-0 (Figures S5D and 5E); this enhanced SA level in BIK1$^{S89D/T90D}$ as early as 24 hpi is consistent with enhanced bacterial resistance in this mutant even at 24 hpi (Figure S4E).

We next examined the expression of SA- and JA-responsive genes. Consistent with increased levels of SA and JA in BIK1$^{S89D/T90D}$, both JA-responsive *PDF1.2* and SA-responsive *PR1* were increased in non-infected BIK1$^{S89D/T90D}$ plants (Figures 5F and 5G). Interestingly, we found that at 24 hpi, when both SA and JA are much higher in BIK1$^{S89D/T90D}$ (Figures S5B and S5D), only the high *PR1* level prevails while *PDF1.2* drops to basal level (Figures S5E and S5F). Published studies in *Arabidopsis* where SA and methyl JA are applied simultaneously also show similar pattern of prevalence of *PR1* over *PDF1.2* (Koornneef et al., 2008; Spoel et al., 2003). Together these results demonstrate that *Pst* DC3000 induces JA and SA levels through BIK1 and provide a mechanistic link between bacterial resistance and downstream hormone regulation.

BIK1 Localizes to the Nucleus, and Interacts and Transphoshorylates WRKY TFs

Next, we explored the mechanisms of how BIK1 regulates JA and SA. JA is a lipid-derived signaling molecule involved in the regulation of various stress responses in plants (Wasternack and Song, 2017). JA synthesis is initiated in chloroplasts from polyunsaturated fatty acids and completed in peroxisomes. A GH3 family protein jasmonate resistant 1 (JAR1) conjugates JA to isoleucine to produce bioactive JA-Ile. The major regulation of JA pathway occurs in the nucleus through ZIM domain containing JAZ and WRKY TFs (Birkenbihl et al., 2012; Gao et al., 2011; Jiang and Yu, 2016; Wasternack and Song, 2017).

However, BIK1 has not been shown to localize to any organelle associated with JA signaling. BIK1 was initially identified as a plasma membrane localized protein, based on transient overexpression of BIK1 in onion cells by particle bombardment (Veronese et al., 2006). In order for BIK1 to directly regulate JA response, BIK1 must be present beyond the plasma membrane; preferentially in the nucleus, chloroplast, or peroxisome.

We first investigated BIK1 localization to the nucleus because major regulation of JA occurs in the nucleus. We used percoll-based gradient fractionation (Folta and Kaufman, 2006) of stable *Arabidopsis* transgenic plants expressing BIK1^{WT}-HA under native BIK1 promoter to enrich intact nuclear fractions without contamination from the plasma membrane or other organelles. We found that BIK1 was highly enriched in the nuclear fraction compared with cytoplasmic (phosphoenolpyruvate carboxylase, PEPC), plasma membrane (FLS2), thylakoid (LHCII type I chlorophyll a/b-binding protein, LHCB1) or stroma (Rubisco large subunit, RBCL) fractions (Figures 6A and 6B). To further validate the biochemical fractionation results, we expressed BIK1 fused to tagCFP (BIK1-tCFP) in *Nicotiana benthamiana* leaves and observed under confocal microscope. BIK1-tCFP localizes to the nucleus in addition to the plasma membrane (Figure 6C). Western blot analysis of tissue used for microscopy revealed that tCFP was not cleaved, ruling out the possibility that cleaved tCFP was localizing to the nucleus (Figure 6D). Localization of BIK1 was not altered by S89A/T90A or S89D/T90D mutations (Figures S6A and S6B). Together these data reveal that BIK1 localizes to both plasma membrane and nucleus.

Next, we tested how BIK1 in the nucleus might be regulating JA. Various WRKY TFs have been shown to modulate JA responses (Gao et al., 2011; Jiang and Yu, 2016). It has been shown that WRKY33, 50, 51, and 57 play an important role in JA signaling (Gao et al., 2011; Jiang and Yu, 2016). WRKY33, 50, and 51 are also implicated in SA regulation (Birkenbihl et al., 2012; Gao et al., 2011). We used bimolecular fluorescence complementation assay in *N. benthamiana* to determine the interaction between BIK1 with WRKY33, 50, 51, and 57. Co-expression of BIK1 fused to the N-terminal 155 amino acid residues of citrine (BIK1^{YN}) and WRKY33, 50, or 57 fused to the C terminus of citrine (WRKY33^{YC}, WRKY50^{YC}, and WRKY57^{YC}) reconstituted citrine fluorescence but not in tissues co-expressing BIK1^{YN} with WRKY51^{YC} or NLS-GUS^{YC} control (Figure 6E). These results indicate that BIK1 interacts with WRKY33, 50, and 57 in the nucleus. We further validated these results by co-immunoprecipitation assay using BIK1 transiently expressed in *N. benthamiana* and purified GST-tagged WRKY proteins from bacteria (Figure 6F). Interestingly, BIK1$^{S89D/T90D}$ had weaker in teractions, while BIK1$^{S89A/T90A}$ had stronger interaction with WRKY33, 50, and 57 (Figure 6F). These results are consistent with our observation that modification of the electrostatic charge surrounding the S89/T90 region of BIK1 has important functional connotation by altering the physical interaction between BIK1 and downstream signaling proteins.

We next tested if BIK1 can trans-phosphorylate these WRKYs. Consistent with the interaction data, BIK1 can selectively transphosphorylate WRKY33, 50, and 57, but not 51 (Figure 6G). A kinase-dead version of BIK1 was unable to trans-phosphorylate WRKY33, 50, and 57 (Figure S6C). Since BIK1's auto-phosphor-ylation activity is not altered by S89A/T90A or S89D/T90D (Figure S4C), we tested if BIK1's trans-phosphorylation activity

toward WRKYs is altered by these mutations. We found that BIK1$^{S89D/T90D}$ has significantly reduced trans-phosphorylation toward WRKY57, 50, and 33 compared with BIK1^{WT} and BIK1$^{S89A/T90A}$ (Figures 6H, S6D, and S6E). We next tested if reduced trans-phosphorylation of BIK1$^{S89D/T90D}$ was specific to WRKY or other BIK1 trans-phosphorylation targets also reduced by BIK1$^{S89D/T90D}$. RBOHD is membrane-localized protein involved in ROS generation during PTI (Nühse et al., 2007) and BIK1 trans-phosphorylate the N terminus of RBOHD (RBOHD_N) (Kadota et al., 2014; Li et al., 2014). BIK1's ability to trans-phosphorylate RBOHD_N was not altered by BIK1$^{S89D/T90D}$ (Figure 6I). Together these results demonstrate that BIK1 specifically trans-phosphorylates WRKY33, 50, and 57, and that the trans-phosphorylation ability of BIK1 is selectively impaired toward WRKYs by phosphomimetic mutation at S89/T90 residues.

DISCUSSION

EFR Regulates JA in Response to Bacterial Infection

EFR and FLS2 PRRs interact with co-receptor BAK1 and intra-cellular BIK1 RLCK during the immune response against bacterial pathogens. The BAK1 association with PRR is dependent on the presence of PAMPs that bring the extracellular LRR domain of PRR and BAK1 in close proximity and help to form a PRRBAK1 complex (Sun et al., 2013). In contrast, BIK1 constitutively associates with PRR and dissociates after PAMP perception (Lu et al., 2010; Zhang et al., 2010). BIK1 is rapidly phosphorylated after PAMP perception, which is dependent on the kinase activity of BAK1 and PRRs (Lu et al., 2010). BAK1 trans-phosphorylates BIK1 on conserved sites in the activation loop that is mostly responsible for regulating the kinase activity of BIK1 (Lin et al., 2014). On the other hand, the relationship between PRRs and BIK1 in terms of phosphorylation was until now unclear.

Here, we show that the kinase domain of EFR purified from the insect cell expression system can directly phosphorylate BIK1 *in vitro*. Since the kinase domain of PRR purified from the bacterial expression system possesses no trans-phosphorylation activity (Lu et al., 2010; Schwessinger et al., 2011), an insect cell or other eukaryotic expression system might be a better system for studying PRR-mediated trans-phosphorylation of previously identified interactors of PRRs. Loss-of-function phosphonull mutants of these sites (BIK1$^{S89A/T90A}$) abolished elf18 sensitivity, indicating that these phosphorylation sites are important for activating EFR-mediated immune signaling. Interestingly, gain-of-function phosphomimetic mutant (BIK1$^{S89D/T90D}$) plants showed hypersensitivity toward elf18-mediated responses. The crystal structure of BIK1 revealed that the S89/T90 residues are present in a uniquely extended "open flower" shaped loop, which might provide an interface for protein-protein interaction. Furthermore, the presence of Asp and Glu at 87 and 88 positions, respectively, gives a partial negative charge to this region. Therefore, phosphorylation of S89 and T90 or mutations of these residues to aspartic acid alters the local charge of this region and will affect protein-protein interaction, which is dependent on this region. We observed weaker interaction between EFR and BIK1$^{S89D/T90D}$ than between EFR and BIK1^{WT}, even in the absence of elf18, suggesting that interaction of EFR with BIK1 is dependent on the electrostatic charge of this region.

Significant progress has been made in understanding the role of plant hormones in defense against pathogens (Pieterse et al., 2012; Robert-Seilaniantz et al., 2011). Hormone regulation after PAMP perception is well established; however, the mechanism underlying hormone regulation post-PAMP perception remains largely unknown. JA and ET have been shown to be involved in providing resistance against necrotrophic pathogens (Berrocal-Lobo et al., 2002; Glazebrook, 2005; Pieterse et al., 2012; Robert-Seilaniantz et al., 2011). The role of JA against biotrophic and hemibiotrophic pathogens has not been established previously. Until recently, it was generally accepted that SA and JA have mutually exclusive roles in defense against biotrophic versus necrotrophic pathogens (Glaze-brook, 2005; Spoel et al., 2007). Recent systems biology approaches and network analysis have revealed a previously unrecognized collaborative role between JA and SA during biotrophic and hemibiotrophic pathogen defense (Hillmer et al., 2017; Kim et al., 2014; Tsuda et al., 2009). Direct hormone measurement with higher-order mutations of JA, SA, ET, and phytoalexin deficient 4 (PAD4) signaling networks has revealed that the JA subnetwork positively regulates both SA- and PAD4-mediated signaling, which is important for defense against biotrophic pathogens (Hillmer et al., 2017). More recently, it was shown that both JA and SA could exist in an elevated state during effector-triggered immunity (Liu et al., 2016). These and other results show that mere presence of higher level of one hormone is not responsible for the reduced level of other hormone and a more complex regulation lies underneath the SA and JA dichotomy. Our results show that hemibiotrophic pathogen *Pst* DC3000 infection leads to increased JA and SA levels, and that BIK1 plays an important role in regulation of these hormones during EFR signaling. BIK1$^{S89D/T90D}$ phosphomimetic mutant for EFR sites have increased JA and SA levels, even in the absence of bacterial infection. Furthermore, both JA and SA levels further increased significantly after bacterial infection in BIK1$^{S89D/T90D}$ phosphomimetic mutants. Consequently these mutants are more resistant to bacteria and their resistance increases if the plants were primed for EFR signaling. Our findings establish a direct mechanistic link between PRR-mediated immune signaling and hormone regulation through BIK1 RLCK.

BIK1's Nuclear Role

Transcriptional reprogramming is a hallmark of PRR signaling as most of the events on the plasma membrane during PAMP perception ultimately lead to changes in the transcription of immune-related genes (Li et al., 2016). Activation of MAPKs during PRR signaling is a well-studied pathway that establishes a link between PRR activation and transcriptional reprogramming. However, players that connect PRR to MAPK activation and pathways that regulate transcription independent of MAPK cascade during PRR signaling remain elusive. Hormone regulation during PRR signaling also depends on transcriptional changes; however, the proteins and pathways linking these transcriptional changes directly to PRR activation also remain largely unknown. Here, we identified a new pathway that connects EFR to downstream hormone regulation through BIK1 during bacterial infection. We found that BIK1 localizes to the nucleus in addition to the plasma membrane. These findings indicate that BIK1 may directly control various transcription-regulated processes during PRR signaling (Figure 7).

WRKY TFs play important role in regulating gene expression during immune signaling (Tsuda and Somssich, 2015). WRKY33, 50, 51, and 57 in particular have been attributed toward regulation of JA and SA (Birkenbihl et al., 2012; Gao et al., 2011; Jiang and Yu, 2016). WRKY50 and 51 have been shown to be positive regulators of SA-mediated signaling and are responsible for SA-mediated suppression of JA signaling (Gao et al., 2011). On the other hand, WRKY33 has been shown to negatively regulate SA-mediated responses (Birkenbihl et al., 2012). Our finding that BIK1 can interact and phosphorylate WRKY33, 50, and 57 establishes a direct role for BIK1 in the nucleus. $BIK1^{S89D/T90D}$ phosphomimetic mutant, which shows increased JA and SA levels, also has weak interaction and reduced trans-phosphorylation ability toward WRKY57, 33, and 50. Protein interaction and phosphorylation can have both positive and negative effects on downstream regulation. Since WRKY57 and 50 have been shown to be negative regulators of JA, it is possible that BIK1-mediated phosphorylation of WRKY57 and 50 could negatively regulate JA. In $BIK1^{S89D/T90D}$ mutant, where BIK1 has reduced trans-phosphorylation toward WRKY57 and 50, we observed decreased negative regulation of JA (Figure 7). WRKY33 has been shown to be a negative regulator of SA signaling as *wrky33* plants show inappropriate activation of SA responses (Birkenbihl et al., 2012). Interestingly, $BIK1^{S89D/T90D}$ mutant has increased SA, while, biochemically, $BIK1^{S89D/T90D}$ protein has reduced trans-phosphorylation to ward WRKY33. These results suggest that BIK1-mediated phosphorylation of WRKY33 might negatively regulate SA. Based on these findings, we hypothesize that, in non-infected wild-type plants, BIK1 interacts and phosphorylates WRKY33. During infection BIK1 gets phosphorylated at S89/T90, which results in reduced interaction and trans-phosphorylation of WRKY33, and therefore is unable to inhibit SA induction (Figure 7).

A Role for RLCKs Beyond Plasma Membrane?

RLCKs are released from plasma membrane-localized PRR complexes to activate downstream signaling during PTI (Lin et al., 2014; Lu et al., 2010; Zhang et al., 2010). However, their downstream targets, and function beyond the plasma membrane, are not known. Our results showing nuclear localization of BIK1 and its interaction with WRKY TFs reveal a role for RLCK family protein beyond plasma membrane in immune signaling. It will be interesting in the future to test if other SA and JA transcriptional regulators interact with BIK1 and if they are targets of BIK1 trans-phosphorylation. The *Arabidopsis* genome contains ~ 160 RLCKs, and some of them are known to play regulatory roles in growth and defense (Lehti-Shiu et al., 2009). BSK1 RLCK plays an essential role in brassinosteroid-mediated growth signaling. Upon brassinosteroid perception, BRI1 forms a complex with BAK1 and phosphorylates BSK1, which in turn interacts with downstream phosphatase BSU1. BSK1 interaction with BSU1 leads to dephosphorylation of BZR1 and BES1 TF. In light of BIK1 localization to the nucleus, it will be interesting to test if BSK1 also plays a direct role in the nucleus during BR signaling.

RLCK members PBL1, PBS1, PBL13, PBL27, and RIPK play specific roles during immunity against various pathogens (Tang et al., 2017). Signaling through these RLCKs ultimately culminates in the nucleus. It will be interesting in the future to determine if other

RLCK members also localize to the nucleus and play a direct role inside the nucleus during immune signaling.

STAR★METHODS

KEY RESOURCES TABLE

REAGENT or RESOURCE	SOURCE	IDENTIFIER
Antibodies		
Rabbit polyclonal anti-pS/T	Abcam	Cat#ab17464; RRID:AB_443891
Mouse monoclonal anti-HIS	Sigma	Cat#H1029; RRID:AB_260015
Mouse monoclonal anti-HA	Sigma	Cat# H6908; RRID:AB_260070
Mouse monoclonal anti-GST	SantaCruz	Cat# SC374171; RRID:AB_11008206
Rabbit polyclonal anti-FLS2	Agrisera	Cat# AS121857
Rabbit polyclonal anti-PEPC	abcam	Cat#ab34793; RRID:AB_777192
Rabbit polyclonal anti-Histone H3	abcam	Cat#ab1791; RRID:AB_302613
Rabbit polyclonal anti-Lhcb1	Agrisera	Cat#AS09 522; RRID:AB_10507202
Rabbit polyclonal anti-Rbcl	Agrisera	Cat# AS03 037A; RRID:AB_2175288
Rabbit polyclonal anti-FLAG	Sigma	Cat#F1804; RRID:AB_262044
Rabbit polyclonal anti-pMAPK	Cell Signaling	Cat#9101; RRID:AB_331646
Bacteria and Virus Strains		
High5	ThermoFisher	Cat#B85502
SF-9	ThermoFisher	Cat#11496015
Agrobacterium tumefaciens GV3101	Holsters et al., 1980	N/A
Escherichia coli BL21	NEB	Cat# C25271
Escherichia coli DH5α	ThermoFisher	Cat#18258012
Pseudomonas syringae pv tomato (Pst) DC3000	N/A	N/A
Chemicals, Peptides, and Recombinant Proteins		
Glutathione Sepharose 4 (affinity gel)	ThermoFisher	Cat#16100
Cobalt affinity column	ThermoFisher	Cat#89965
1-aminocyclopropane-1-carboxylic acid (ACC)	Sigma	Cat#A3903
Protease inhibitor cocktail	Sigma	Cat#P9599
cOmplete mini EDTA-free protease inhibitor cocktail	Roche	Cat# 11836170001
Phusion High-Fidelity DNA Polymerase	ThermoFisher	Cat#F549L
elf18 peptide	Ezbiolab	Cat#cp7211
iTaq Universal SYBR Green Supermix	BioRad	Cat#1725122
Protease Inhibitor Cocktail Tablets	Roche	Cat#04693116001
Trizol	Life Technologies	Cat#10296–028
Superscript III Reverse Transcriptase	Life Technologies	Cat#18080044
Oligo(dT)$_{12–18}$ primer	ThermoFisher	Cat#18418012
DNase I (RNase-free)	New England Biolabs	Cat#M0303S
Glufocinate-Ammonium	Sigma	Cat#45520
ExpressiveFive media	ThermoFisher	Cat#10486025
SF-900 III SFM media	ThermoFisher	Cat#12658027
RNase Out	Life Technologies	Cat#10777–019
Critical Commercial Assays		

REAGENT or RESOURCE	SOURCE	IDENTIFIER
Zymoclean Gel DNA Recovery Kit - Uncapped columns	Zymo Research Corporation	Cat#D4002
DNA Clean & Concentrator-5 - Uncapped Columns	Zymo Research Corporation	Cat#D4004
ZR Plasmid Miniprep-Classic Kit	Zymo Research Corporation	Cat#D4016
Deposited Data		
BIK1 Crystal Structure	RCSB Protein Data Bank	PDB: 5tos
Experimental Models: Organisms/Strains		
Arabidopsis:pBIK1-BIK1$^{S89A/T90A}$-HA	This paper	N/A
Arabidopsis:pBIK1-BIK1$^{S89D/T90D}$-HA	This paper	N/A
Arabidopsis:pBIK1-BIK1^{T120A}-HA	This paper	N/A
Arabidopsis: pBIK1-BIK1^{S129A}-HA	This paper	N/A
Arabidopsis:pBIK1-BIK1$^{T120A/S129A}$-HA	This paper	N/A
Nicotiana benthamiana	Taxonomy ID: 4100	N/A
Oligonucleotides		
See Table S2		
Recombinant DNA		
pBIK1-BIK1$^{S89A/T90A}$-HA	This paper	N/A
pBIK1-BIK1$^{S89D/T90D}$-HA	This paper	N/A
pBIK1-BIK1^{T120A}-HA	This paper	N/A
pBIK1-BIK1^{S129A}-HA	This paper	N/A
pBIK1-BIK1$^{T120A/S129A}$-HA	This paper	N/A
His-GST-TEV-BIK1	This paper	N/A
His-GST-TEV-BIK1	This paper	N/A
His-TEV-EFR-CD (Insect cell expression)	This paper	N/A
His-TEV-EFR-CD* (Insect cell expression)	This paper	N/A
His-TEV-EFR-CDΔJM (Insect cell expression)	This paper	N/A
His-TEV-BIK1	This paper	N/A
His-TEV-BIK1$^{S89A/T90A}$	This paper	N/A
His-TEV-BIK1^{S89DT90D}	This paper	N/A
His-GST-TEV-WRKY33	This paper	N/A
His-GST-TEV-WRKY50	This paper	N/A
His-GST-TEV-WRKY51	This paper	N/A
His-GST-TEV-WRKY57	This paper	N/A
pUBQ-BIK1-tagCFP-HA	This paper	N/A
pUBQ-BIK1$^{S89A/T90A}$-tagCFP-HA	This paper	N/A
$_{P}$UBQ-BIK1$^{S89D/T90D}$-tagCFP-HA	This paper	N/A
pNOS-BIK1^{YN}	This paper	N/A
pNOS-WRKY33^{YC}	This paper	N/A
pNOS-WRKY50^{YC}	This paper	N/A
pNOS-WRKY51^{YC}	This paper	N/A
pNOS-WRKY57^{YC}	This paper	N/A
pNOS-NLS-GUS^{YC}	This paper	N/A

REAGENT or RESOURCE	SOURCE	IDENTIFIER
Software and Algorithms		
Prism 7	GraphPad	RRID:SCR_002798

CONTACT FOR REAGENT AND RESOURCE SHARING

Further information and requests for resources and reagents should be directed to and will be fulfilled by the Lead Contact, Savithramma P. Dinesh-Kumar (spdineshkumar@ucdavis.edu).

EXPERIMENTAL MODEL AND SUBJECT DETAILS

Plants

Arabidopsis: Wild-type *Arabidopsis* accession Col-0 and *bik1* mutant (Lu et al., 2010; Veronese et al., 2006) were used in this study. Col-0, *bik1*, BIK1^{WT}, BIK1$^{S89A/T90A}$ and BIK1$^{S89D/T90D}$ plants were grown under short day condition (10 h light/14 h dark) or under long day condition (16 h light/8 h dark). Transgenic plants were generated using floral dip method (Clough and Bent, 1998). pBIK1:BIK1$^{S89A/T90A}$- 3xHA and pBIK1:BIK1$^{S89D/T90D}$-3xHA, pBIK1:BIK1^{T120A}-3xHA, pBIK1:BIK1^{S129A}-3xHA and pBIK1:BIK1$^{T120A/S129A}$-3xHA plasmids were generated using isothermal assembly and sequenced to confirm the plasmids. Agrobacterium strain GV3101 was transformed with different plasmids and selected on LB agar plates with appropriate antibiotics. 200ml of agrobacterium culture was grown overnight and harvested by centrifugation. Pelleted cells were resuspended with sterilized water with 0.02% Silwet L77 and diluted to OD_{600} of 1. Flowering *Arabidopsis bik1* plants with clipped primary bolts and small secondary bolts with few open flowers were dipped in agrobacterium solution for 20 seconds (3 times). Seeds from dipped plants were harvested after 4 weeks and called T_0. Positive transformants were selected on MS plate with Glufocinate-Ammonium, transplanted onto soil and seeds from these plants were called T_1. All experiments were conducted with T_2 plants.

Nicotiana benthamiana: *N. benthamiana* was grown in growth chamber at 22°C with a long-day photoperiod (16 h light and 8 h dark).

Bacterial Strains—*Pst* DC3000 and *hrcC* mutant were grown at 28°C on the King's B (KB) medium with appropriate antibiotics.

Insect Cells—Sf-9 cells were maintained at 23°C incubator in spinner flask in Sf-900 II SFM media. High5 cells were maintained at 23°C incubator in Expressive SFM media.

METHOD DETAILS

Expression of EFR_CD in Insect Cell Expression System—EFR_CD (691–1032 amino acids), EFR-CD*(kinase dead), EFR_CDΔJM (675–1031 amino acids) proteins were purified from insect cell expression system. Briefly, these inserts were cloned into a modified bac-to-bac baculovirus expression vector in-frame with an N-terminal 6xHIS tag followed by TEV cleavage site. Recombinant virus was generated by infecting Sf-9 cells in

6 well-plate and virus titer was determined. Virus was amplified to MOI of 3. Recombinant protein was expressed by infecting 500ml of Hi5 cells with amplified virus. 72 h after infection, cells were harvested by centrifugation and lysed using a douncer in 50ml of lysis buffer (15mM HEPES, 150mM NaCl, 10mM imidazole, 2mM mercaptaethanol, pH7.3). Cell debris and insoluble material was separated by centrifugation at 50,000×g for 15 min at 4°C. Protein was purified using Cobalt affinity column (ThermoFisher). The column was washed with 20ml of lysis buffer before eluting with 4 column volume of elution buffer (20mM HEPES, 120mM NaCl, 250mM imidazole, pH7.3). The elution from cobalt column was loaded on to a Superdex S200(16/60) size exclusion column equilibrated with 20mM HEPES, 200mM NaCl, pH7.3. Peak fraction from size exclusion column was separated on SDS-PAGE and stained with coomassie blue to conform the purity of protein. Protein was concentrated and stored at −80°C.

Bacterial Protein Expression and Crystallization of BIK1—Full-length BIK1 was amplified from *Arabidopsis* Col-0 cDNA library and was cloned into *E. coli* expression vector with an N-terminal 6xHIS-tag followed by TEV cleavage site using isothermal assembly. The plasmid was sequenced to confirm the clone. BIK1 expression and purification was performed as described in (Lal et al., 2016). Briefly, 12L 2XYT media was inoculated with overnight grown $(HIS)_6$-TEV-BIK1 BL21 culture. BIK1 was purified by 3-step purification strategy of affinity chromatography followed by ion exchange and size exclusion chromatography. HIS-tag was cleaved by incubating with TEV protease followed by affinity and size exclusion chromatography. BIK1 crystallization was performed as described previously using batch method (Lal et al., 2016).

BIK1 Structure Determination—X-ray diffraction data were collected on beamline 12–2 at Stanford Synchrotron Radiation Lightsource to 2.35Å resolution (Table S1). The BIK1 structure was solved by Molecular Replacement using an ensemble of kinase structures in the PHENIX program (Adams et al., 2010). The ensemble of structures included BAK1 (PDBID: 3uim), BRI1 (PDBID: 4oh4), IRAK4 (PDBID: 2nru), and tomato protein kinase Pto (PDBID: 2qkw). The BIK1 structure was modeled using the program COOT (Emsley and Cowtan, 2004) and refined against PHENIX (Afonine et al., 2012). Table S1 lists the statistics for data processing and structure refinement. The final R-factor and R-free vales are 23.8 and 26.8, respectively.

Mass Spectrometry—Equal amount of purified kinase-dead BIK1 was incubated with purified EFR in kinase buffer (30mM Tris, 150mM NaCl, 1mM ATP, 5mM $MgCl_2$, 3mM $MnCl_2$, pH7.3) for 1 h and separated by SDS-PAGE. The gel was stained with coomassie brilliant blue (CBB) stain and the protein bands were sliced for mass spectrometry sample processing. The gel pieces were washed with ammonium bicarbonate followed by acetonitrile, the samples were reduced by incubating with 10mM DTT in 50mM ammonium bicarbonate for 30 min at 56°C. The gel pieces were washed again with acetonitrile to remove DTT. Cysteine residues were carbamidomethylated by incubation with 55mM iodoacetamide in 50mM ammonium bicarbonate for 20 min in dark. Iodoacetamide was removed and samples were incubated with trypsin in ammonium bicarbonate and incubated overnight at 37°C. LC-MS/MS was performed using nanoflow-HPLC and Q-Exactive

hybrid quadruple-Orbitrap at UC Davis Genome Center proteomics facility (http://proteomics.ucdavis.edu/). The protein identification searches were performed on a directed basis using TAIR 10 *Arabidopsis* protein database (www.arabidopsis.org) by TurboSEQUEST via the BioWorks interface and then imported into Scaffold. Within Scaffold, spectra were searched with X¸Tandem. Carbamidomethylation of Cys residues were specified as a fixed modification and oxidized Met and phosphorylation of Ser, Thr, or Tyr residues were allowed as variable modifications. The predicted phosphorylation sites were manually confirmed before acceptance.

Seedling Growth Inhibition Assay—Seeds were surface sterilized using ethanol and spotted on 1/2 MS plates with 0.5% sucrose. To synchronize germination, seeds were stratified at 4°C for 4 days. Seeds were grown under short day condition for additional 6 days. Individual seedlings were transferred to a single well of 48 well-plate containing either MS media alone or with 1μM elf18. Fresh weight of 10 days old individual seedling was measured using precision scale. Eight replicates of each genotype were measured for statistical analysis and experiment was repeated five times. Statistical analysis was performed using GraphPad Prism 7 software.

Bacteria Growth Assay—*Pseudomonas syringae* pv *tomato* (*Pst*) DC3000 growth assay was performed by syringe inoculation in *Arabidopsis*. *Pst* DC3000 was grown on LB agar plate with 50 μg/ml rifampicin for 48 h at 28°C. Bacteria was scraped from the plates and resuspended in 10mM $MgCl_2$. The bacterial resuspension was diluted to OD_{600} of 0.001 or 1×10^5 colony-forming units (cfu)/mL and hand inoculated using a needle-less syringe onto 4–5 week old plants. To access if pre-activation of PAMP-triggered immunity (PTI) inhibit bacterial growth, 4–5 week old *Arabidopsis* plants were pre-inoculated with 100nM of elf18 or H_2O 24 h prior to *Pst* DC3000 infection. Plants were grown for 3 additional days in short day chamber. Three leaf discs from different plants per genotype were collected and homogenized in 10mM $MgCl_2$ using beat beater. Serial dilutions of homogenized samples were plated on LB agar plate with appropriate antibiotics. Data were graphed with triplicate values and each experiment was repeated at least three times. Statistical analysis was performed using GraphPad Prism 7 software.

MAPK Assay—3–4 week old plants were treated with 1μM of elf 18 and tissue was collected at 0, 10, 30 and 120 min and flash frozen in liquid nitrogen. The samples were grounded in liquid nitrogen and resuspended in extraction buffer {30mM Tris, 150 mM NaCl, 0.2% triton X-100, 1mM NaF, 1X PhosSTOP (Roche), 1x cOmplete protease inhibitor (Roche)}. Equal amount of protein was loaded on SDS-PAGE gel based on Bradford assay. Proteins were transferred to nitrocellulose membrane and incubated with p44/42 MAPK antibody (#9101; Cell Signalling) overnight.

Hormone Measurement—Leaves were weighed and frozen in liquid nitrogen. Immediately after freezing tissue was homogenized in a paint shaker for 20 sec. Following homogenization, frozen tissue was extracted as previously described (Casteel et al., 2015). For analysis, 5 mL of each extract was analyzed using a Thermo Electron LTQ-Orbitrap XL Hybrid MS. Samples were separated on a Zorbax Extend-C18 HPLC column (Phenomenex

Kinetex, 5 μm, 100 × 2.10 mm) using 0.1% formic acid in water (Solvent A) and 0.1% (v/v) formic acid in acetonitrile (Solvent B) at a flow rate of 300 μL min–1. The gradient used was 0–0.5 min, 20% B; 0.5–13.5 min, linear gradient to 100% B; 13.6–17 min, linear gradient to 30% B; 17.1–18 min, linear gradient to 20% B.

Quantitative Real-Time PCR—Leaf tissues were collected from non-infected and infected plants at indicated time points and total RNA was extracted using TRIzol reagent (Life Technologies) by following the manufacturer's protocol. Total RNA was treated with DNase I RNase free (New England Biolabs) and cDNA was synthesized using SuperScript III reverse transcriptase (Life Technologies) and oligo(dT)12–18 primer by following the manufacturer's protocol. Real-time qRT-PCR was performed using Bio-Rad CFX96 qPCR instrument (Bio-Rad) using iTaq Universal SYBR Green Supermix (Bio-Rad) and 2.5 mM each gene specific primers listed in Key Resources Table and 5% diluted cDNA. Data presented are normalized for UBQ5 expression level.

Nuclear Fractionation—Nuclear fractionation was performed using percoll based gradient. 2 grams of leaves were chopped with a razor blade and homogenized in 4ml of extraction buffer (2.0 M hexylene glycol (2-methyl-2,4-pentandiol), 40 mM HEPES-KOH pH 7.8, 10 mM $MgCl_2$ and 5 mM 2-mercaptoethanol) using motor and pestle. Homogenate was filtered through 100μm cell strainer (Falcon 352360). Triton X-100 was added to a final concentration of 1%. Percoll gradient was set up as described and nuclei were enriched at the interface of 30% and 80% Percoll. Enriched nuclei were washed with extraction buffer and centrifuges at 1000g to pellet the nuclei. Purity of nuclei was confirmed by western blot analyses against plasma membrane specific α-FLS2, cytoplasmic specific α-PEPC, nucleus specific α-Histone H3, thylakoids LHCII type I chlorophyll a/b-binding protein (LHCB1) or stroma Rubisco large subunit (RBCL) antibody.

Localization, BiFC, and Microscopy—For localization, BIK1 was fused to tagCFP under the control of Arabidopsis UBQ10 promoter and a NOS terminator. For BiFC, BIK1 was fused to the N-terminal 155 amino acid residues of citrine (YN) and WRKY33, WRKY50, WRKY 51, WRKY57, and NLS-GUS were fused to the C-terminal of citrine (YC) under the control of a NOS promoter and a NOS terminator. These plasmids were transformed into Agrobacterium strain GV3101. Agrobacterium-mediated transient expressions in *N. benthamiana* leaves were performed as described in (Padmanabhan et al., 2013). For localization, OD_{600} = 0.2 and for BiFC, OD_{600} = 0.5 was used. For BiFC, Agrobacterium containing YN and YC constructs were co-infiltrated at 1:1 ratio. Fluorescence imaging was performed using Zeiss 710 Laser scanning confocal system using an Axio observer Z1 inverted microscope with 40X/1.2 NA C-Apochromat water immersion objective. Approximately, 4 mm^2 *N. benthamiana* leaf sections were excised 48 hours after transient expression. The 458 nm and 514 nm laser lines of a 25 mW Argon laser (Coherent) with appropriate emission filters were used to image tagCFP and Citrine with chloroplast. Alternatively, a 458 nm laser line of a 25 mW Argon laser and a META detector was used for chloroplast autofluorescence.

Protoplast Isolation, Plasmid Transfection and Coimmunoprecipitation—The protoplast isolation, transfection and Co-IP assays were reported previously (Lu et al., 2010). Briefly, 500 mL of protoplasts at a density of 2×10^5/mL were transfected with EFR-FLAG or a control vector without EFR (C) and HA-tagged BIK1 or different BIK1 mutants. Six hours after transfection, protoplasts were treated with mock (−) or with 1 mM elf18 (+) for 15 min, and collected for Co-IP assay. Protoplasts were lysed with 0.5 ml of extraction buffer (10 mM HEPEs, pH7.5, 100 mM NaCl, 1 mM EDTA, 10% Glycerol, 0.5% Triton X-100 and protease inhibitor cocktail from Roche), and the samples were centrifuged at 13,000 rpm for 10 min at 4°C. The supernatant was incubated with a-FLAG agarose for 2 hr at 4°C with gentle shaking. The beads were collected and washed three times with washing buffer (10 mM HEPEs, pH7.5, 100 mM NaCl, 1 mM EDTA, 10% Glycerol, and 0.1% Triton X-100), and once with 50 mM Tris-HCl, pH7.5. The immunoprecipitated proteins were analyzed by western blot with an a-HA or a-FLAG antibody.

QUANTIFICATION AND STATISTICAL ANALYSIS

All the quantification and statistical parameters are mentioned in the figure legends. Quantification of immunoblot data in Figure 6B is from two independent experiments and data was analyzed with Image J software (National Institutes of Health). The data are presented as mean ± SEM. For the pathogen infection assays, n represents the number of samples in each replicate. Statistical significance between two groups were analyzed by ANNOVA/Dunnette's multiple comparison, and asterisks indicate the statistical significance mentioned in figure legends for each experiment. At least three biological replicates were included. Statistical analysis was performed by GraphPad Prism 7.

DATA AND SOFTWARE AVAILABILITY

The BIK1 crystal structure is deposited in the RCSB Protein Data Bank under PDB ID 5tos.

Supplementary Material

Refer to Web version on PubMed Central for supplementary material.

ACKNOWLEDGMENTS

This work is supported by UC Davis Research Investments in Science and Engineering (RISE) (to S.P.D.-K. and A.J.F.) and NSF-IOS-1354434 (to S.P.D.-K.). N.K.H. and A.J.F. were partially supported by NIH training grant T32 GM007377 and by National Institute of Food and Agriculture (NIFA) grant CA-D-MCB-2310-H, respectively. Use of the Stanford Synchrotron Radiation Lightsource, SLAC National Accelerator Laboratory, is supported by the U.S. Department of Energy, Office of Science, Office of Basic Energy Sciences under contract no. DE-AC02–76SF00515. The SSRL Structural Molecular Biology Program is supported by the DOE Office of Biological and Environmental Research, and by the NIH, National Institute of General Medical Sciences (including P41GM103393). We thank Professor George Bruening for coordinating the RISE project at UC Davis. We thank Tesfaye Mengiste and Chris Staiger for *bik1* seeds and Barry Chan for help in the generation of transgenic lines. We thank UC Davis Genome Center Proteomics Core Facility and Brett Phinney and Anthony Herren.

REFERENCES

Adams PD, Afonine PV, Bunkoczi G, Chen VB, Davis IW, Echols N, Headd JJ, Hung LW, Kapral GJ, Grosse-Kunstleve RW, et al. (2010). PHENIX: a comprehensive Python-based system for macromolecular structure solution. Acta Crystallogr. D Biol. Crystallogr 66, 213–221. [PubMed: 20124702]

Afonine PV, Grosse-Kunstleve RW, Echols N, Headd JJ, Moriarty NW, Mustyakimov M, Terwilliger TC, Urzhumtsev A, Zwart PH, and Adams PD (2012). Towards automated crystallographic structure refinement with phenix.refine. Acta Crystallogr. D Biol. Crystallogr 68, 352–367. [PubMed: 22505256]

Berrocal-Lobo M, Molina A, and Solano R (2002). Constitutive expression of ETHYLENE-RESPONSE-FACTOR1 in *Arabidopsis* confers resistance to several necrotrophic fungi. Plant J. 29, 23–32. [PubMed: 12060224]

Birkenbihl RP, Diezel C, and Somssich IE (2012). *Arabidopsis* WRKY33 is a key transcriptional regulator of hormonal and metabolic responses toward *Botrytis cinerea* infection. Plant Physiol. 159, 266–285. [PubMed: 22392279]

Casteel CL, De Alwis M, Bak A, Dong H, Whitham SA, and Jander G (2015). Disruption of ethylene responses by turnip mosaic virus mediates suppression of plant defense against the green peach aphid vector. Plant Physiol. 169, 209–218. [PubMed: 26091820]

Clough SJ, and Bent AF (1998). Floral dip: a simplified method for *Agrobacterium*-mediated transformation of *Arabidopsis thaliana*. Plant J. 16, 735–743. [PubMed: 10069079]

Couto D, and Zipfel C (2016). Regulation of pattern recognition receptor signalling in plants. Nat. Rev. Immunol 16, 537–552. [PubMed: 27477127]

Emsley P, and Cowtan K (2004). Coot: model-building tools for molecular graphics. Acta Crystallogr. D Biol. Crystallogr 60, 2126–2132. [PubMed: 15572765]

Felix G, Duran JD, Volko S, and Boller T (1999). Plants have a sensitive perception system for the most conserved domain of bacterial flagellin. Plant J. 18, 265–276. [PubMed: 10377992]

Flury P, Klauser D, Schulze B, Boller T, and Bartels S (2013). The anticipation of danger: microbe-associated molecular pattern perception enhances AtPep-triggered oxidative burst. Plant Physiol. 161, 2023–2035. [PubMed: 23400703]

Folta KM, and Kaufman LS (2006). Isolation of *Arabidopsis* nuclei and measurement of gene transcription rates using nuclear run-on assays. Nat. Protoc 1, 3094–3100. [PubMed: 17406505]

Gao QM, Venugopal S, Navarre D, and Kachroo A (2011). Low oleic acid-derived repression of jasmonic acid-inducible defense responses requires the WRKY50 and WRKY51 proteins. Plant Physiol. 155, 464–476. [PubMed: 21030507]

Glazebrook J (2005). Contrasting mechanisms of defense against biotrophic and necrotrophic pathogens. Annu. Rev. Phytopathol 43, 205–227. [PubMed: 16078883]

Gómez-Gómez L, Bauer Z, and Boller T (2001). Both the extracellular leucine-rich repeat domain and the kinase activity of FSL2 are required for flagellin binding and signaling in Arabidopsis. Plant Cell 13, 1155–1163. [PubMed: 11340188]

Gómez-Gómez L, and Boller T (2000). FLS2: an LRR receptor-like kinase involved in the perception of the bacterial elicitor flagellin in *Arabidopsis*. Mol. Cell 5, 1003–1011. [PubMed: 10911994]

Hanks SK, and Hunter T (1995). Protein kinases 6. The eukaryotic protein kinase superfamily: kinase (catalytic) domain structure and classification. FASEB J. 9, 576–596. [PubMed: 7768349]

Hillmer RA, Tsuda K, Rallapalli G, Asai S, Truman W, Papke MD, Sakakibara H, Jones JDG, Myers CL, and Katagiri F (2017). The highly buffered *Arabidopsis* immune signaling network conceals the functions of its components. PLoS Genet. 13, e1006639. [PubMed: 28472137]

Holsters M, Silva B, Van Vliet F, Genetello C, De Block M, Dhaese P, Depicker A, Inze D, Engler G, Villarroel R, et al. (1980). The functional organization of the nopaline *A. tumefaciens* plasmid pTiC58. Plasmid 3, 212–230. [PubMed: 6100894]

Huse M, and Kuriyan J (2002). The conformational plasticity of protein kinases. Cell 109, 275–282. [PubMed: 12015977]

Jeffrey PD, Russo AA, Polyak K, Gibbs E, Hurwitz J, Massague J, and Pavletich NP (1995). Mechanism of CDK activation revealed by the structure of a cyclinA-CDK2 complex. Nature 376, 313–320. [PubMed: 7630397]

Jiang Y, and Yu D (2016). The WRKY57 transcription factor affects the expression of jasmonate ZIM-domain genes transcriptionally to compromise *Botrytis cinerea* resistance. Plant Physiol. 171, 2771–2782. [PubMed: 27268959]

Kadota Y, Sklenar J, Derbyshire P, Stransfeld L, Asai S, Ntoukakis V, Jones JD, Shirasu K, Menke F, Jones A, et al. (2014). Direct regulation of the NADPH oxidase RBOHD by the PRR-associated kinase BIK1 during plant immunity. Mol. Cell 54, 43–55. [PubMed: 24630626]

Kim Y, Tsuda K, Igarashi D, Hillmer RA, Sakakibara H, Myers CL, and Katagiri F (2014). Mechanisms underlying robustness and tunability in a plant immune signaling network. Cell Host Microbe 15, 84–94. [PubMed: 24439900]

Koornneef A, Verhage A, Leon-Reyes A, Snetselaar R, Van Loon L, and Pieterse CM (2008). Towards a reporter system to identify regulators of cross-talk between salicylate and jasmonate signaling pathways in *Arabidopsis*. Plant Signal. Behav 3, 543–546. [PubMed: 19513248]

Lal NK, Fisher AJ, and Dinesh-Kumar SP (2016). *Arabidopsis* receptor-like cytoplasmic kinase BIK1: purification, crystallization and X-ray diffraction analysis. Acta Crystallogr. F Struct. Biol. Commun 72, 738–742. [PubMed: 27710938]

Laluk K, Luo H, Chai M, Dhawan R, Lai Z, and Mengiste T (2011). Biochemical and genetic requirements for function of the immune response regulator BOTRYTIS-INDUCED KINASE1 in plant growth, ethylene signaling, and PAMP-triggered immunity in *Arabidopsis*. Plant Cell 23, 2831–2849. [PubMed: 21862710]

Lehti-Shiu MD, Zou C, Hanada K, and Shiu SH (2009). Evolutionary history and stress regulation of plant receptor-like kinase/pelle genes. Plant Physiol. 150, 12–26. [PubMed: 19321712]

Li B, Meng X, Shan L, and He P (2016). Transcriptional regulation of pattern-triggered immunity in plants. Cell Host Microbe 19, 641–650. [PubMed: 27173932]

Li J, Wen J, Lease KA, Doke JT, Tax FE, and Walker JC (2002). BAK1, an *Arabidopsis* LRR receptor-like protein kinase, interacts with BRI1 and modulates brassinosteroid signaling. Cell 110, 213–222. [PubMed: 12150929]

Li L, Li M, Yu L, Zhou Z, Liang X, Liu Z, Cai G, Gao L, Zhang X, Wang Y, et al. (2014). The FLS2-associated kinase BIK1 directly phosphorylates the NADPH oxidase RbohD to control plant immunity. Cell Host Microbe 15, 329–338. [PubMed: 24629339]

Lin W, Li B, Lu D, Chen S, Zhu N, He P, and Shan L (2014). Tyrosine phosphorylation of protein kinase complex BAK1/BIK1 mediates *Arabidopsis* innate immunity. Proc. Natl. Acad. Sci. USA 111, 3632–3637. [PubMed: 24532660]

Liu L, Sonbol FM, Huot B, Gu Y, Withers J, Mwimba M, Yao J, He SY, and Dong X (2016). Salicylic acid receptors activate jasmonic acid signalling through a non-canonical pathway to promote effector-triggered immunity. Nat. Commun 7, 13099. [PubMed: 27725643]

Lu D, Wu S, Gao X, Zhang Y, Shan L, and He P (2010). A receptor-like cytoplasmic kinase, BIK1, associates with a flagellin receptor complex to initiate plant innate immunity. Proc. Natl. Acad. Sci. USA 107, 496–501. [PubMed: 20018686]

Mishina TE, and Zeier J (2007). Pathogen-associated molecular pattern recognition rather than development of tissue necrosis contributes to bacterial induction of systemic acquired resistance in *Arabidopsis*. Plant J. 50, 500–513. [PubMed: 17419843]

Nam KH, and Li J (2002). BRI1/BAK1, a receptor kinase pair mediating brassinosteroid signaling. Cell 110, 203–212. [PubMed: 12150928]

Nühse TS, Bottrill AR, Jones AM, and Peck SC (2007). Quantitative phosphoproteomic analysis of plasma membrane proteins reveals regulatory mechanisms of plant innate immune responses. Plant J. 51, 931–940. [PubMed: 17651370]

Padmanabhan MS, Ma S, Burch-Smith TM, Czymmek K, Huijser P, and Dinesh-Kumar SP (2013). Novel positive regulatory role for the SPL6 transcription factor in the N TIR-NB-LRR receptor-mediated plant innate immunity. PLoS Pathog. 9, e1003235. [PubMed: 23516366]

Pieterse CM, Van der Does D, Zamioudis C, Leon-Reyes A, and Van Wees SC (2012). Hormonal modulation of plant immunity. Annu. Rev. Cell Dev. Biol 28, 489–521. [PubMed: 22559264]

Postel S, Küfner I, Beuter C, Mazzotta S, Schwedt A, Borlotti A, Halter T, Kemmerling B, and Nürnberger T (2010). The multifunctional leucine-rich repeat receptor kinase BAK1 is implicated in *Arabidopsis* development and immunity. Eur. J. Cell Biol. 89, 169–174. [PubMed: 20018402]

Ranf S, Eschen-Lippold L, Frohlich K, Westphal L, Scheel D, and Lee J (2014). Microbe-associated molecular pattern-induced calcium signaling requires the receptor-like cytoplasmic kinases, PBL1 and BIK1. BMC Plant Biol. 14, 374. [PubMed: 25522736]

Robert X, and Gouet P (2014). Deciphering key features in protein structures with the new ENDscript server. Nucleic Acids Res. 42, W320–W324. [PubMed: 24753421]

Robert-Seilaniantz A, Grant M, and Jones JD (2011). Hormone crosstalk in plant disease and defense: more than just jasmonate-salicylate antagonism. Annu. Rev. Phytopathol 49, 317–343. [PubMed: 21663438]

Schwessinger B, Roux M, Kadota Y, Ntoukakis V, Sklenar J, Jones A, and Zipfel C (2011). Phosphorylation-dependent differential regulation of plant growth, cell death, and innate immunity by the regulatory receptor-like kinase BAK1. PLoS Genet. 7, e1002046. [PubMed: 21593986]

Spoel SH, Johnson JS, and Dong X (2007). Regulation of tradeoffs between plant defenses against pathogens with different lifestyles. Proc. Natl. Acad. Sci. USA 104, 18842–18847. [PubMed: 17998535]

Spoel SH, Koornneef A, Claessens SM, Korzelius JP, Van Pelt JA, Mueller MJ, Buchala AJ, Métraux JP, Brown R, Kazan K, et al. (2003). NPR1 modulates cross-talk between salicylate- and jasmonate-dependent defense pathways through a novel function in the cytosol. Plant Cell 15, 760–770. [PubMed: 12615947]

Sun Y, Li L, Macho AP, Han Z, Hu Z, Zipfel C, Zhou JM, and Chai J (2013). Structural basis for flg22-induced activation of the *Arabidopsis* FLS2-BAK1 immune complex. Science 342, 624–628. [PubMed: 24114786]

Tang D, Wang G, and Zhou JM (2017). Receptor kinases in plant-pathogen interactions: more than pattern recognition. Plant Cell 29, 618–637. [PubMed: 28302675]

Thiel KW, and Carpenter G (2007). Epidermal growth factor receptor juxta-membrane region regulates allosteric tyrosine kinase activation. Proc. Natl. Acad. Sci. USA 104, 19238–19243. [PubMed: 18042729]

Tsuda K, Sato M, Stoddard T, Glazebrook J, and Katagiri F (2009). Network properties of robust immunity in plants. PLoS Genet. 5, e1000772. [PubMed: 20011122]

Tsuda K, and Somssich IE (2015). Transcriptional networks in plant immunity. New Phytol. 206, 932–947. [PubMed: 25623163]

Veronese P, Nakagami H, Bluhm B, Abuqamar S, Chen X, Salmeron J, Dietrich RA, Hirt H, and Mengiste T (2006). The membrane-anchored BOTRYTIS-INDUCED KINASE1 plays distinct roles in *Arabidopsis* resistance to necrotrophic and biotrophic pathogens. Plant Cell 18, 257–273. [PubMed: 16339855]

Wasternack C, and Song S (2017). Jasmonates: biosynthesis, metabolism, and signaling by proteins activating and repressing transcription. J. Exp. Bot 68, 1303–1321. [PubMed: 27940470]

Wei L, Hubbard SR, Smith RF, and Ellis L (1994). Protein kinase super-family — comparisons of sequence data with three-dimensional structures. Curr. Opin. Struct. Biol 4, 450–455.

Yan L, Ma Y, Liu D, Wei X, Sun Y, Chen X, Zhao H, Zhou J, Wang Z, Shui W, et al. (2012). Structural basis for the impact of phosphorylation on the activation of plant receptor-like kinase BAK1. Cell Res. 22, 1304–1308. [PubMed: 22547027]

Zhang J, Li W, Xiang T, Liu Z, Laluk K, Ding X, Zou Y, Gao M, Zhang X, Chen S, et al. (2010). Receptor-like cytoplasmic kinases integrate signaling from multiple plant immune receptors and are targeted by a *Pseudomonas syringae* effector. Cell Host Microbe 7, 290–301. [PubMed: 20413097]

Zipfel C, Kunze G, Chinchilla D, Caniard A, Jones JD, Boller T, and Felix G (2006). Perception of the bacterial PAMP EF-Tu by the receptor EFR restricts *Agrobacterium*-mediated transformation. Cell 125, 749–760. [PubMed: 16713565]

Zipfel C, Robatzek S, Navarro L, Oakeley EJ, Jones JD, Felix G, and Boller T (2004). Bacterial disease resistance in *Arabidopsis* through flagellin perception. Nature 428, 764–767. [PubMed: 15085136]

Highlights

- The immune receptor EFR phosphorylates BIK1 at S89/T90 in a unique extended loop
- BIK1 S89/T90 are required for EFR-mediated defense responses
- Defense phytohormones JA and SA are elevated in BIK1 phosphomimetic mutant plants
- BIK1 localizes to the nucleus and targets WRKY transcription factors to regulate JA/SA

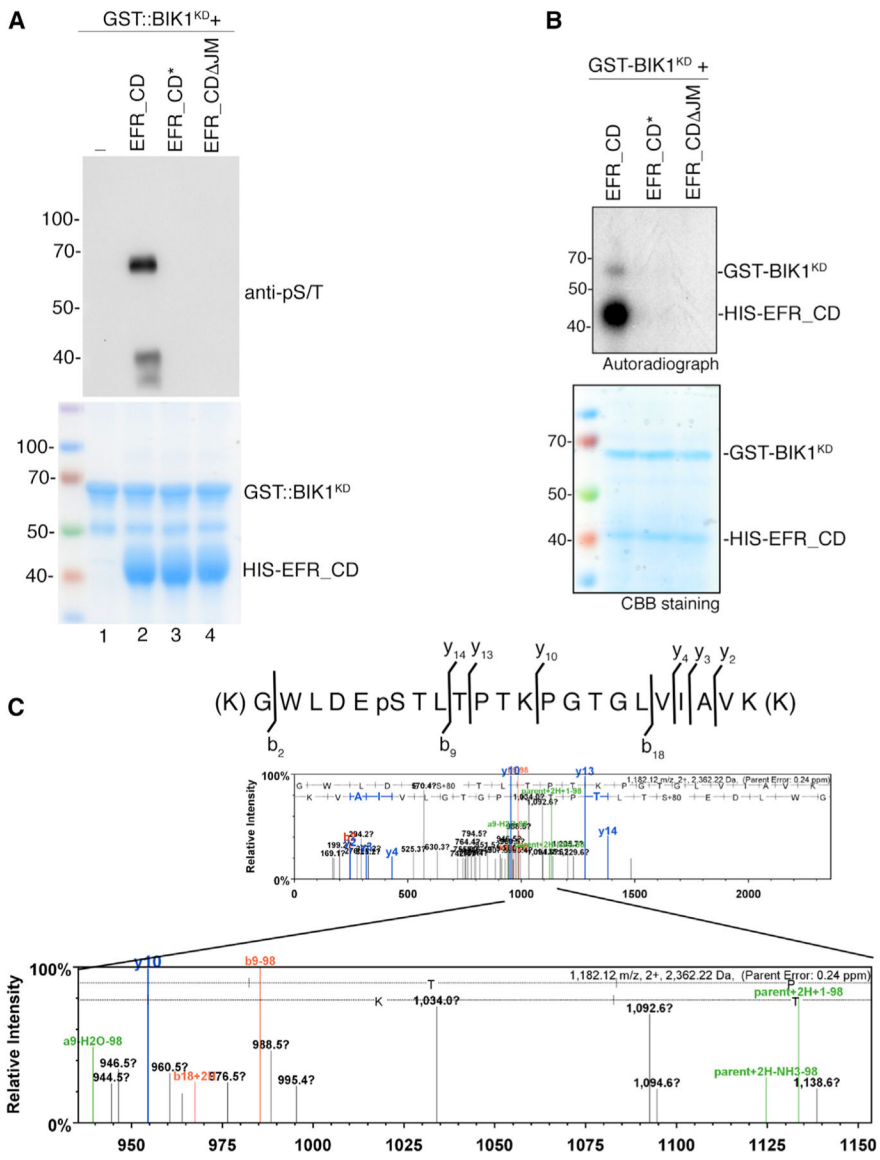

Figure 1. EFR Cytoplasmic Kinase Domain Trans-Phosphorylates BIK1 at S89/T90 Residues

(A) *In vitro* EFR auto-phosphorylation and EFR trans-phosphorylation of BIK1. Auto-phosphorylation activity (top panel) of insect cell purified $(HIS)_6$-tagged EFR cytoplasmic kinase domain (EFR_CD), kinase-dead mutant (EFR_CD*), and EFR_CD lacking juxtamembrane (JM) region (EFR_CDDJM). Trans-phosphorylation activity of insect cell purified EFR_CD, EFR_CD* and EFR_CDΔJM on $(HIS)_6$-GST-tagged kinase-dead BIK1 (GST::$BIK1^{KD}$) purified from *E. coli* (top panel). Phosphorylation was detected using anti-pS/T antibody. Coomassie-stained gel shows GST::$BIK1^{KD}$, EFR_CD, EFR_CD*, and EFR_ CDDJM proteins (bottom panel). Protein sizes marked on the left are in kDa. Numbers on the bottom refer to lanes 1–4.

(B) *In vitro* radioactive-based EFR trans-phosphorylation assay. HIS-tagged EFR_CD, EFR_CD*, or EFR_CDΔJM purified from insect cell and GST-tagged BIK1 purified from *E. coli* were incubated with [$\gamma-^{32}$P]ATP. Phosphorylation was detected by autoradiography. CBB,

Coomassie brilliant blue. Protein sizes marked on the left are in kDa. Similar results were obtained in two independent experiments.

(C) EFR_CD phosphorylates BIK1 at S89/T90 residues. Mass spectrometry analyses of BIK1 phosphorylated sites by EFR_CD. The b and y ions are marked in spectra with respective peptide sequence above the spectrum. Neutral loss of a phosphate group with mass of 98 Da is indicated.

See also Figure S1.

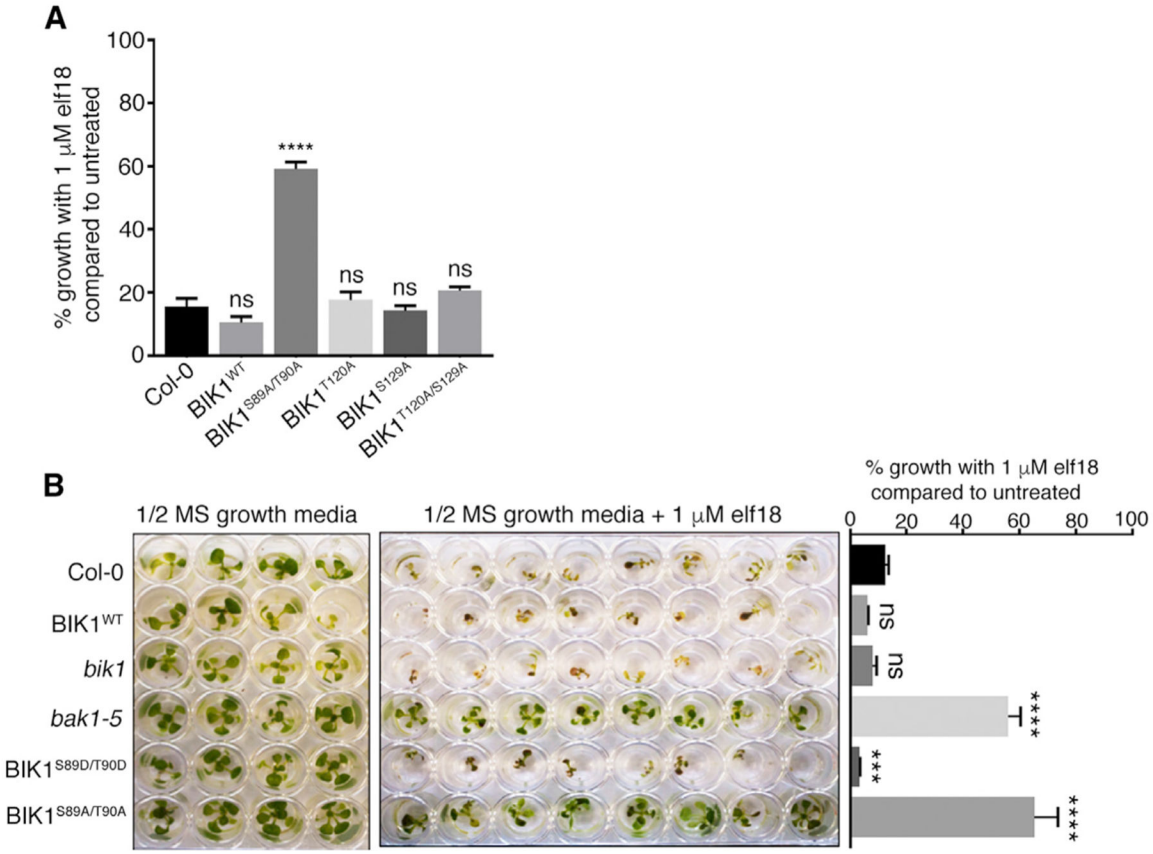

Figure 2. BIK1 S89 and T90 Are Important for EFR-Mediated Growth Inhibition Response to elf18 Ligand

(A) Mutations in S89/T90 of BIK1 rescues seedling growth suppression mediated by elf18 ligand. Fresh weight of seedlings of wild-type *Arabidopsis* Col-0 and *bik1* complemented with wild-type BIK1 ($BIK1^{WT}$), BIK1 S89A/T90A ($BIK1^{S89A/T90A}$), BIK1 T120A ($BIK1^{T120A}$), BIK1 S129A ($BIK1^{S129A}$), and BIK1 T120A/S129A ($BIK1^{T120A/S129A}$) in the presence of 1 mM elf18. The data were normalized against control Col-0 as reference (mean ± SD; n > 8; ****p < 0.0001; ns, not significant, ANOVA/Dunnett's multiple comparison test). Similar results were obtained in three independent experiments.

(B) Seedling growth sensitivity assay of wild-type Col-0, *bak1–5*, *bik1*, and *bik1* complemented with $BIK1^{WT}$, $BIK1^{S89D/T90D}$, and $BIK1^{S89A/T90A}$ in the absence (left panel) and in the presence of 1 μM elf18 (middle panel). Quantitation (right panel) of fresh weight of seedlings in the middle panel normalized against control (mean ± SD; n > 8; ****p < 0.0001, ***p = 0.0002; ns, not significant, ANOVA/Dunnett's multiple comparison test). Similar results were obtained in three independent experiments.

See also Figure S2.

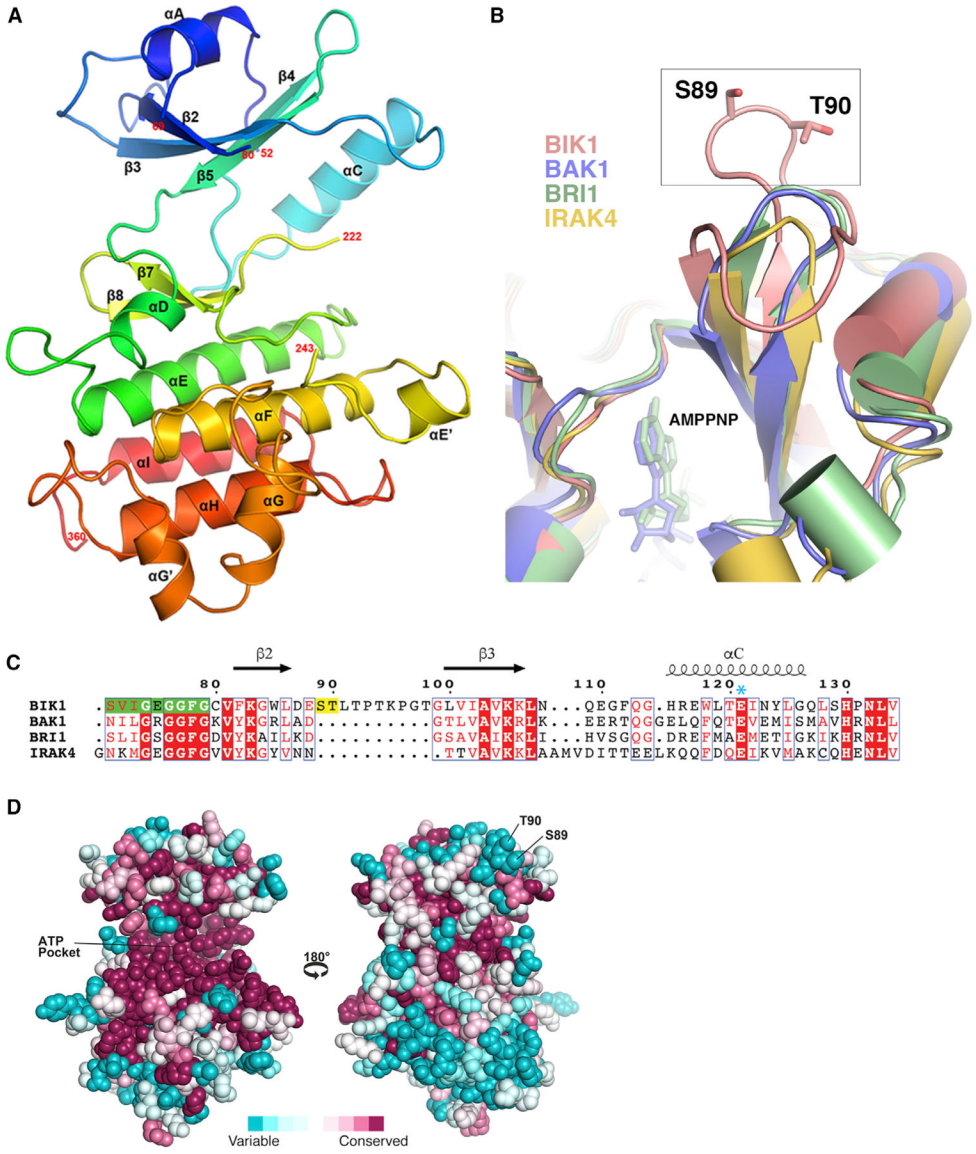

Figure 3. BIK1 Crystal Structure Reveals BIK1 S89 and T90 in a Unique Extended Loop

(A) Crystal structure of BIK1 monomer colored by the rainbow spectrum; N terminus (blue), and C terminus (red). Secondary structure elements labeled based on cyclin-dependent kinase (CDK) topology.

(B) The β2-β3 loop, which contains S89 and T90, is uniquely extended in BIK1 compared with closely related kinases. The structures superimpose onto BIK1 with a root-mean-square deviation of 1.30Å for BAK1, 1.07Å for BRI1, and 1.11Å for IRAK4, comparing 198, 171, and 183 equivalent a carbons, respectively.

(C) Sequence alignment around the β2-β3 loop and helix αC comparing the similar kinases. Residues highlighted in green are disordered in the BIK1 structure, yellow highlighted residues correspond to S89 and T90, and the catalytically important Glu in αC is marked by a cyan asterisk.

(D) Space-filling representation of the BIK1 structure colored according to sequence conservation of kinases. Generated by the program ConSurf.
See also Figure S3 and Table S1.

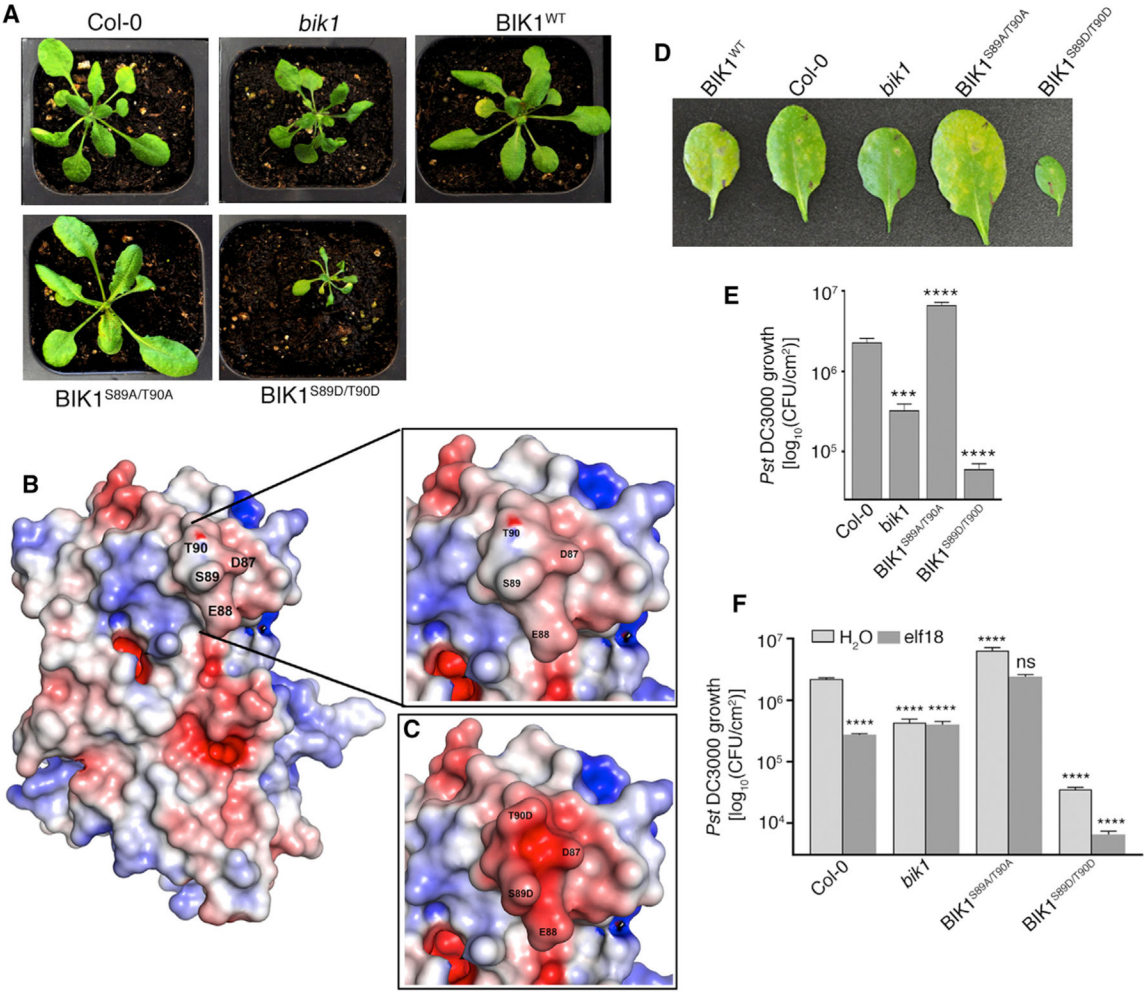

Figure 4. BIK1$^{S89A/T90A}$ Phospho-Null and BIK1$^{S89D/T90D}$ Phospho-Mimetic Mutants Have Opposite Effects on Growth and Defense

(A) Growth phenotypes of wild-type Col-0 compared with *bik1* and *bik1* complemented with BIK1^{WT}, BIK1$^{S89A/T90A}$, and BIK1$^{S89D/T90D}$. Photographs were taken 22 days after germination. Similar phenotypes were observed in multiple plants (Figure S4) and in three different lines.

(B) Electrostatic surface potential of BIK1 with positively (blue) and negatively (red) charged regions. Zoomed region surrounding BIK1 S89 and T90 (right panel).

(C) Hypothetical electrostatic charge of the region surrounding S89 and T90 in BIK1$^{S89D/T90D}$.

(D) Disease symptoms 3 days after syringe inoculation of *Pst* DC3000. Similar results were obtained in three independent experiments.

(E) Colony-forming units (CFU) of *Pst* DC3000 bacteria from (D). Mean ± SD; n > 3; ****p < 0.0001, ***p < 0.001, ANOVA/Dunnett's multiple comparison test compared with Col-0. Similar results were obtained in three independent experiments.

(F) CFU of *Pst* DC3000 3 days after syringe inoculation of leaves pre-treated with 100 nM elf18 or H_2O for 24 hr (mean ± SD; n > 3; ****p < 0.0001, ANOVA/Dunnett's multiple

comparison test) compared with mock-treated Col-0. Similar results were obtained in three independent experiments.
See also Figure S4.

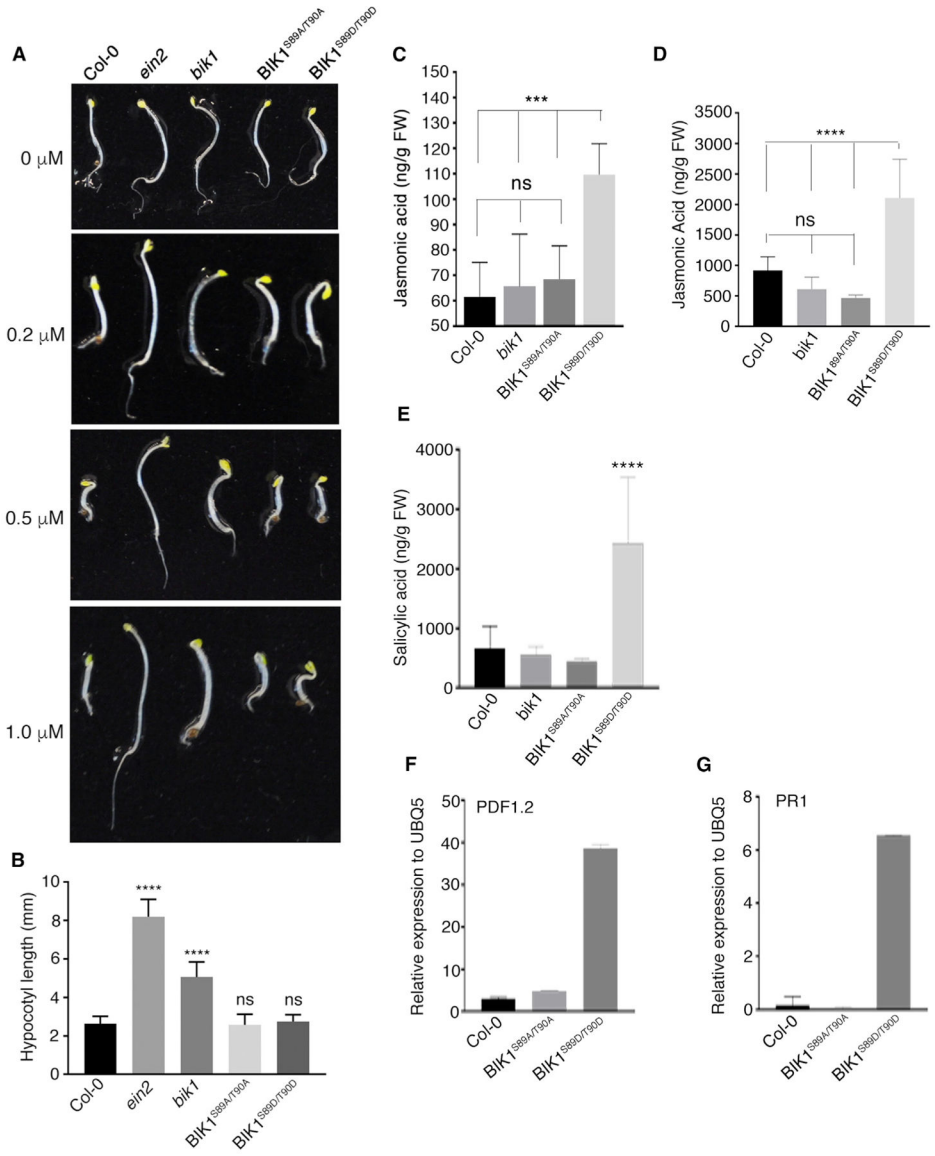

Figure 5. BIK1$^{S89D/T90D}$ Accumulates Higher Levels of JA

(A) BIK1$^{S89A/T90A}$ and BIK1$^{S89D/T90D}$ have no effect on ethylene response. BIK1$^{S89A/T90A}$ and BIK1$^{S89D/T90D}$ restore *bik1* insensitivity to ethylene similar to that of Col-0 wild-type.

(B) Hypocotyl length quantification of seedlings from (A); mean ± SD; n > 15. Statistical analysis was performed with ANOVA/Dunnett's multiple comparison test compared with Col-0; ****p < 0.0001; ns, not significant.

(C and D) JA levels were increased in 3-week-old BIK1$^{S89D/T90D}$ plants compared with wild-type Col-0, *bik1*, and BIK1$^{S89A/T90A}$ plants (C). JA levels were further increased in BIK1$^{S89D/T90D}$ plants 2 days after syringe inoculation with *Pst* DC3000 (D). mean ± SD; n = 8. ***p < 0.001 in (C) and ****p < 0.0001 in (D), statistical analysis was performed with ANOVA/Dunnett's multiple comparison test compared with BIK1$^{S89D/T90D}$; p = ns when Col-0 was used as a control. Similar results were obtained in three independent experiments.

(E) SA levels were increased 2 days after syringe inoculation with *Pst* DC3000 in BIK1$^{S89D/T90D}$ plants compared with wild-type Col-0, *bik1*, and BIK1$^{S89A/T90A}$ plants. Mean ± SD; n = 8. Statistical analysis was performed with ANOVA/Dunnett's multiple comparison test compared with Col-0; ****p < 0.0001; ns, not significant.
(F and G) JA-responsive *PDF1.2* (F) and SA-responsive *PR1* (G) genes are upregulated in BIK1$^{S89D/T90D}$ plants compared with wild-type Col-0 and BIK1$^{S89A/T90A}$ plants. qRT-PCR was performed using *UBQ5* as a reference. Data from three biological replicates were combined and values are shown as mean ± SD.
See also Figure S5.

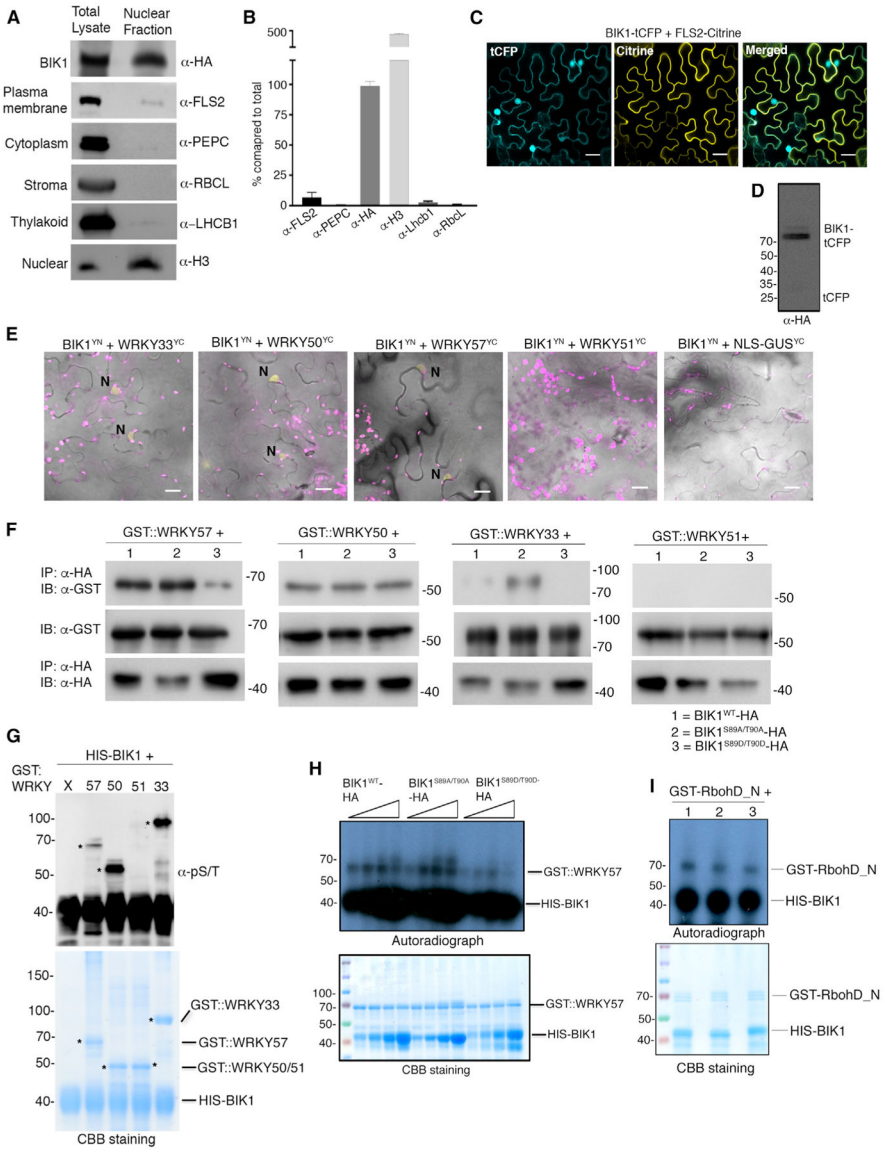

Figure 6. BIK1 Localizes to the Nucleus to Regulate JA Signaling by Targeting WRKY Proteins

(A) Nuclear fractionation of BIK1-HA transgenic *Arabidopsis* plants. BIK1-HA was detected in the nuclear fraction (panel 1). FLS2 as a plasma membrane (panel 2), PEPC as a cytoplasmic (panel 3), RBCL as a chloroplast stroma (panel 4), LHCB1 as chloroplast thylakoid (panel 5), and histone 3 (H3) as a nuclear (panel 4) markers were used. Similar results were obtained in three independent experiments.

(B) Quantification of protein present in the nuclear fraction compared with total from blots shown in (A).

(C) Co-localization of BIK1-tCFP-HA and FLS2-Citrine in *N. benthamiana* transient assay shows that BIK1 is present both in the nucleus and plasma membrane. Scale bars, 20 μm.

(D) BIK1-tCFP-HA is not cleaved *in planta*. Western blot with a-HA of *N. benthamiana* tissue transiently expressing BIK1-tCFP-HA 48 hr after infiltration. Protein sizes marked on the left are in kDa.

(E) BIK1 interacts with WRKY33, 50, and 57 *in vivo*. Co-expression of BIK1 fused to the N terminus of citrine ($BIK1^{YN}$) with WRKY33, 50, and 57 fused to the C terminus of citrine ($BIK1^{YC}$) in bimolecular fluorescence complementation assay in *N. benthamiana* reconstituted citrine fluorescence in the nucleus (N). Co-expression of $BIK1^{YN}$ with $WRKY51^{YC}$ and $NLS\text{-}GUS^{YC}$ did not reconstitute citrine fluorescence. Scale bars, 20 μm.
(F) BIK1 interacts with WRKY33, 50, and 57 *in vitro*. *N. benthamiana* transiently expressing BIK1-HA was immunoprecipitated with GST-WRKY33, 50, 57, and 51 purified from *E. coli*. *Western* blot was performed with α-HA and α-GST. Protein sizes marked on the right are in kDa.
(G) BIK1 selectively trans-phosphorylate WRKY33, 50, and 57. Trans-phosphorylation activity of HIS-BIK1 purified from *E. coli* on WRKY33, 50, 51, and 57 purified from *E. coli* (top panel). Phosphorylation was detected using anti-pS/T antibody. Coomassie-stained gel shows GST::WRKY33, GST::WRKY50, GST::WRKY51, GST::WRKY57, and HIS-BIK1 (bottom panel). Protein sizes marked on the left are in kDa; asterisks indicate GST::WRKY fusion proteins.
(H) $BIK1^{S89D/T90D}$ has reduced trans-phosphorylation on WRKY57. HIS-tagged $BIK1^{WT}$, $BIK1^{S89A/T90A}$, and $BIK1^{S89D/T90D}$ purified from *E. coli* were incubated with GST-tagged WRKY57 purified from *E. coli*. Phosphorylation was detected by autoradiography with [γ $-^{32}$P]ATP (top panel). Coomassie brilliant blue (CBB)-stained SDS-PAGE gel shows loading of proteins. Protein sizes marked on the left are in kDa. Similar results were obtained in two independent experiments.
(I) $BIK1^{S89A/T90A}$ and $BIK1^{S89D/T90D}$ mutations do not affect trans-phosphorylation of its known target RBOHD N terminus. Trans-phosphorylation of purified RBOHD N terminus (RbohD_N) by $BIK1^{WT}$, $BIK1^{S89A/T90A}$, and $BIK1^{S89D/T90D}$ detected by radioactively labeled [$\gamma-^{32}$P]ATP. Top panel autoradiograph and bottom panel CBB-stained SDS-PAGE gel show loading of proteins. Protein sizes marked on the left are in kDa.
See also Figure S6.

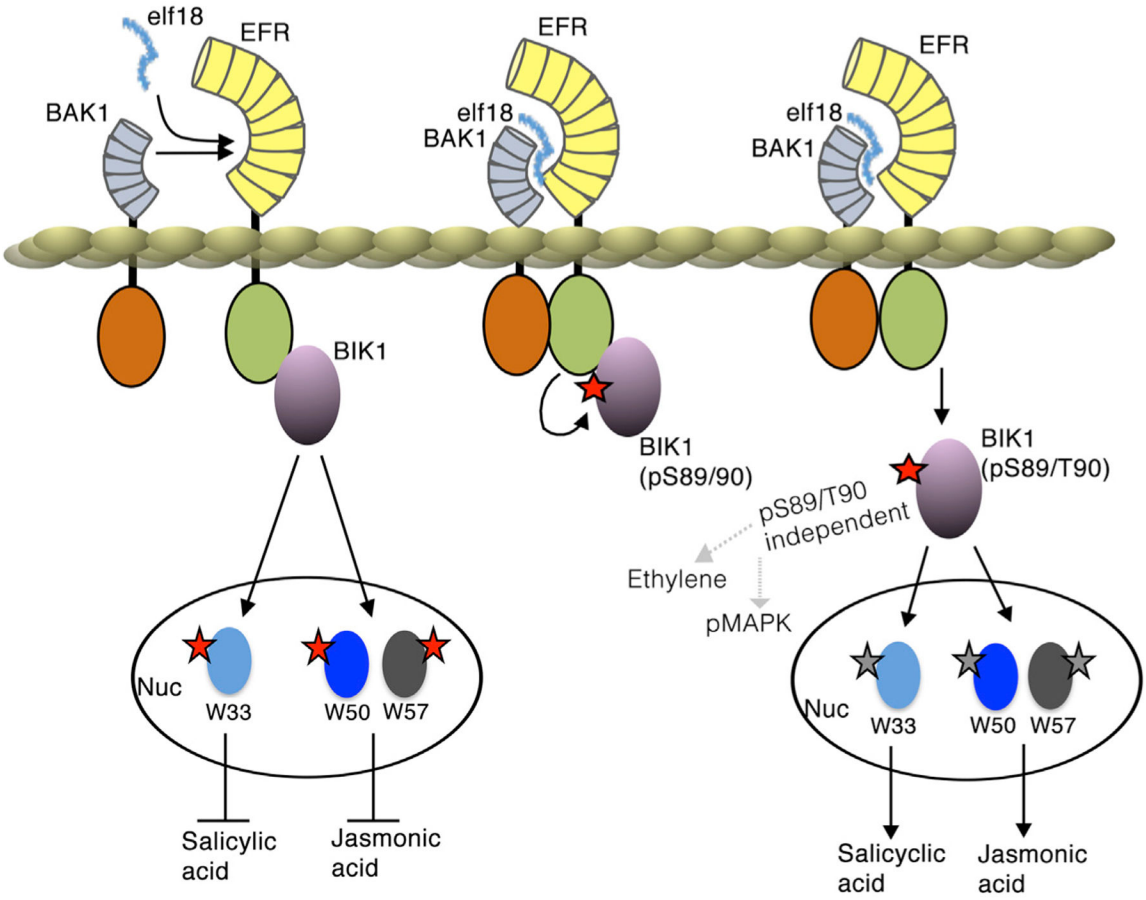

Figure 7. A Proposed Model for the Signal Transduction from EFR to the Nucleus through BIK1 to Modulate JA and SA

A schematic model depicting trans-phosphorylation of BIK1 at S89 and T90 by EFR to activate JA and SA signaling through interaction with WRKY transcription factors in the nucleus (Nuc), independent of ethylene and MAPK cascade. In non-infected cells BIK1 constantly interacts and phosphorylates WRKY33 (W33), WRKY50 (W50), and WRKY57 (W57) to negatively regulate SA and JA. During bacterial infection, BIK1 is phosphorylated at S89/T90 by EFR. Phosphorylation at these sites selectively abolishes BIK1's ability to transphosphorylate WRKYs and consequently results in elevated JA and SA levels.

REAGENT or RESOURCE	SOURCE	IDENTIFIER
Antibodies		
Rabbit polyclonal anti-pS/T	Abcam	Cat#ab17464; RRID:AB_443891
Mouse monoclonal anti-HIS	Sigma	Cat#H1029; RRID:AB_260015
Mouse monoclonal anti-HA	Sigma	Cat# H6908; RRID:AB_260070
Mouse monoclonal anti-GST	SantaCruz	Cat# SC374171; RRID:AB_11008206
Rabbit polyclonal anti-FLS2	Agrisera	Cat# AS121857
Rabbit polyclonal anti-PEPC	abcam	Cat#ab34793; RRID:AB_777192
Rabbit polyclonal anti-Histone H3	abcam	Cat#ab1791; RRID:AB_302613
Rabbit polyclonal anti-Lhcb1	Agrisera	Cat#AS09 522; RRID:AB_10507202
Rabbit polyclonal anti-Rbcl	Agrisera	Cat# AS03 037A; RRID:AB_2175288
Rabbit polyclonal anti-FLAG	Sigma	Cat#F1804; RRID:AB_262044
Rabbit polyclonal anti-pMAPK	Cell Signaling	Cat#9101; RRID:AB_331646
Bacteria and Virus Strains		
High5	ThermoFisher	Cat#B85502
SF-9	ThermoFisher	Cat#11496015
Agrobacterium tumefaciens GV3101	Holsters et al., 1980	N/A
Escherichia coli BL21	NEB	Cat# C25271
Escherichia coli DH5α	ThermoFisher	Cat#18258012
Pseudomonas syringae pv tomato (Pst) DC3000	N/A	N/A
Chemicals, Peptides, and Recombinant Proteins		
Glutathione Sepharose 4 (affinity gel)	ThermoFisher	Cat#16100
Cobalt affinity column	ThermoFisher	Cat#89965
1-aminocyclopropane-1-carboxylic acid (ACC)	Sigma	Cat#A3903
Protease inhibitor cocktail	Sigma	Cat#P9599
cOmplete mini EDTA-free protease inhibitor cocktail	Roche	Cat# 11836170001
Phusion High-Fidelity DNA Polymerase	ThermoFisher	Cat#F549L
elf18 peptide	Ezbiolab	Cat#cp7211
iTaq Universal SYBR Green Supermix	BioRad	Cat#1725122
Protease Inhibitor Cocktail Tablets	Roche	Cat#04693116001
Trizol	Life Technologies	Cat#10296–028
Superscript III Reverse Transcriptase	Life Technologies	Cat#18080044
Oligo$(dT)_{12–18}$ primer	ThermoFisher	Cat#18418012
DNase I (RNase-free)	New England Biolabs	Cat#M0303S
Glufocinate-Ammonium	Sigma	Cat#45520
ExpressiveFive media	ThermoFisher	Cat#10486025
SF-900 III SFM media	ThermoFisher	Cat#12658027
RNase Out	Life Technologies	Cat#10777–019
Critical Commercial Assays		
Zymoclean Gel DNA Recovery Kit - Uncapped columns	Zymo Research Corporation	Cat#D4002

REAGENT or RESOURCE	SOURCE	IDENTIFIER
DNA Clean & Concentrator-5 - Uncapped Columns	Zymo Research Corporation	Cat#D4004
ZR Plasmid Miniprep-Classic Kit	Zymo Research Corporation	Cat#D4016
Deposited Data		
BIK1 Crystal Structure	RCSB Protein Data Bank	PDB: 5tos
Experimental Models: Organisms/Strains		
Arabidopsis:pBIK1-BIK1$^{S89A/T90A}$-HA	This paper	N/A
Arabidopsis:pBIK1-BIK1$^{S89D/T90D}$-HA	This paper	N/A
Arabidopsis:pBIK1-BIK1^{T120A}-HA	This paper	N/A
Arabidopsis: pBIK1-BIK1^{S129A}-HA	This paper	N/A
Arabidopsis:pBIK1-BIK1$^{T120A/S129A}$-HA	This paper	N/A
Nicotiana benthamiana	Taxonomy ID: 4100	N/A
Oligonucleotides		
See Table S2		
Recombinant DNA		
pBIK1-BIK1$^{S89A/T90A}$-HA	This paper	N/A
pBIK1-BIK1$^{S89D/T90D}$-HA	This paper	N/A
pBIK1-BIK1^{T120A}-HA	This paper	N/A
pBIK1-BIK1^{S129A}-HA	This paper	N/A
pBIK1-BIK1$^{T120A/S129A}$-HA	This paper	N/A
His-GST-TEV-BIK1	This paper	N/A
His-GST-TEV-BIK1	This paper	N/A
His-TEV-EFR-CD (Insect cell expression)	This paper	N/A
His-TEV-EFR-CD* (Insect cell expression)	This paper	N/A
His-TEV-EFR-CDΔJM (Insect cell expression)	This paper	N/A
His-TEV-BIK1	This paper	N/A
His-TEV-BIK1$^{S89A/T90A}$	This paper	N/A
His-TEV-BIK1^{S89DT90D}	This paper	N/A
His-GST-TEV-WRKY33	This paper	N/A
His-GST-TEV-WRKY50	This paper	N/A
His-GST-TEV-WRKY51	This paper	N/A
His-GST-TEV-WRKY57	This paper	N/A
pUBQ-BIK1-tagCFP-HA	This paper	N/A
pUBQ-BIK1$^{S89A/T90A}$-tagCFP-HA	This paper	N/A
$_{p}$UBQ-BIK1$^{S89D/T90D}$-tagCFP-HA	This paper	N/A
pNOS-BIK1^{YN}	This paper	N/A
pNOS-WRKY33^{YC}	This paper	N/A
pNOS-WRKY50^{YC}	This paper	N/A
pNOS-WRKY51^{YC}	This paper	N/A
pNOS-WRKY57^{YC}	This paper	N/A
pNOS-NLS-GUS^{YC}	This paper	N/A
Software and Algorithms		

REAGENT or RESOURCE	SOURCE	IDENTIFIER
Prism 7	GraphPad	RRID:SCR_002798